Faculty of Aerospace Engineering

Radar-based landing system for uncontrolled flights

Modifying a collision avoidance radar for synthetic aperture imaging

L. Baardman

September 26, 2016

Delft University of Technology

Challenge the future

Radar-based landing system for uncontrolled flights

Modifying a collision avoidance radar for synthetic aperture imaging

Master of Science Thesis

For obtaining the degree of Master of Science in Aerospace Engineering
at Delft University of Technology

L. Baardman

September 26, 2016

Faculty of Aerospace Engineering · Delft University of Technology

Delft University of Technology

Delft University Of Technology
Department Of
Control and Simulation

The undersigned hereby certify that they have read and recommend to the Faculty of Aerospace Engineering for acceptance a thesis entitled **"Radar-based landing system for uncontrolled flights"** by **L. Baardman** in partial fulfillment of the requirements for the degree of **Master of Science**.

Dated: September 26, 2016

Readers:

Prof.dr.ir. J. M. Hoekstra

Ir. R. N. H. W. van Gent

Dr. Ir. G. N. Saunders

Dr. Ir. J. Ellerbroek

Acronyms

ACC	Area Control Center
AIP	Aeronautical Information Publication
APALS	Autonomous Precision Approach and Landing System
ATC	Air Traffic Control
CAR	Collision Avoidance Radar
CTA	Control Area
CTR	Control Zone
CW	Continuous Wave
DEM	Digital Elevation Map
DFT	Discrete Fourier Transform
DGPS	Differential GPS
DNS	Doppler Navigation System
DUT	Delft University of Technology
FFT	Fast Fourier Transform
FIR	Flight Information Region
FMCW	Frequency Modulated Continuous Wave
GS	Glide Slope
IAS	Indicated Airspeed
ICAO	International Civil Aviation Organization
IFR	Instrument Flight Rules
IMC	Instrument Meteorological Conditions
INS	Inertial Navigation System
LAAS	Local-Area Augmentation System
LOC	Localizer
MSL	Mean Sea Level
NDB	Non-directional Beacon
PBN	Performance Based Navigation

PRI	Pulse Repetition Interval
RMS	Root Mean Square
RNAV	Area Navigation
RNP	Required Navigation Performance
SAR	Synthetic Aperture Radar
SID	Standard Instrument Departure
SNR	Signal-to-Noise
SRTM	Shuttle Radar Topography Mission
STAR	Standard Terminal Arrival Route
TMA	Terminal Control Area
UAC	Upper Area Control Center
UAV	Unmanned Aerial Vehicles
UTA	Upper Control Area
VFR	Visual Flight Rules
VHF	Very High Frequency
VMC	Visual Meteorological Conditions
VOR	VHF Omnidirectional Range
VR	Velocity-Range
WAAS	Wide-Area Augmentation System

Contents

Chapter 1

Abstract

Current aviation regulations allow aircraft to fly under either Visual Flight Rules (VFR) or Instrument Flight Rules (IFR). General aviation aircraft often fly under VFR which exempts these flights from strict regulations concerning flightplanning and aircraft separation by air traffic control services. However, these flights can only be performed with good visibility conditions because aircraft separation relies on pilots seeing each other. IFR allows aircraft to fly under low visibility conditions, but require guidance from air traffic control services for separation and approach and landing procedures.
MetaSensing B.V. in collaboration with Selfly B.V. has developed a Collision Avoidance Radar (CAR) that consists of small, light-weight and low-cost components that ultimately will allow self-separation between aircraft flying under VFR in low visibility conditions. This radar uses Doppler information for detecting objects in the vicinity of the airraft and discern moving objects from the ground. The CAR provides enhanced VFR possibilities in that it allows separation in less than optimal visibility conditions and enhances safety by providing dissimilar redundancy with other avionic systems in self-separation.

The objective of this thesis was to see whether the CAR algorithms could be modified and could be used as a Synthetic Aperture Radar (SAR). SAR can provide high resolution images of the surroundings of an aircraft. This could lead to high precision navigation which offers possibilities for low visibility approach and landing procedures. The limitation of SAR is that it is only able to scan the surroundings sideways of the aircraft, orthonormal to the flight direction, but does so with a high resolution, generally in the order of centimeters for X-band radar systems. Because the SAR can only detect objects such as airport objects and the runway when it is flying by these objects, a navigation system based on this technique is virtually blind on final approach. This means that such a system is dependent on other sources for navigation such as dead-reckoning in the final phase before touchdown. Also, this requires that outside visual information is available before touchdown. This could lead to lateral and longitudinal position errors that need to be corrected for once visual information is available again after descending below the cloud base.

The first part of this research focused on finding the maximum lateral and longitudinal deviations that are acceptable on the final leg of approach in order to land the aircraft safely. In this experiment, participants were asked to fly a VFR circuit towards the runway of a small airport. The visibility conditions used for this experiment were identical to the requirements of a CAT I ILS approach, which means that the cloud base was set at 200 ft. The experiment varied the amount of lateral and longitudinal deviation from the runway centerline at that altitude. When descending below 200 ft the experiment subject was required to perform a correcting manoeuvre due to the lateral and/or longitudinal deviation in order to land the aircraft safely on the runway.
The results show that a lateral deviation of 40 meters required a manoeuvre that is significantly different from the base condition (no lateral/longitudinal deviations). Hence, a radar-based navigation system should provide an accuracy that at least exceeds 40 meters.

Given these results, the second part of this research focused on a computer model of a SAR that meets this accuracy requirement. A SAR module was developed that modifies the CAR in terms of data processing to provide images of the surroundings of the aircraft. A data processing method was developed that uses doppler ranging and interferometry between two antennas to obtain information about the distance and angle of points on the ground relative to the aircraft, and using this method, form an image of the ground contour. A digital elevation model was used as a model of the ground for the radar to detect and the results were compared with the original digital elevation model.
The results showed that an accuracy of 5 meters was achieved which is equal to the theoretical maximum resolution given the radar range resolution that was used. This suggests that the radar is capable of higher resolution when more accurate ground models are used and when more processing power is available.
Even though the simulator experiment shows that an accuracy of better than 40 meters is required, this is easily provided by the SAR model, which provides accuracy levels of a factor 10 better.

The results of the simulator experiment can be enhanced by performing the experiment with more subjects and recalibrate the simulator experiment in order to obtain a more accurate requirement for the allowed deviations. The SAR model relies on several assumptions and is not yet based on real world data for its output. Using experimental data from a real flight could influence the results in terms of accuracy. In conclusion, a radar-based navigation system seems viable for precision navigation applications making CAT I approaches possible for general aviation aircraft without ground support.

Chapter 2

Introduction

The aviation industry can be thought of as consisting of commercial aviation, general aviation and military aviation. The first two groups represent by far the largest portion of all of the aircraft currently in operation. Commercial aviation tries to operate in a profitable and safe manner, using automated navigation systems and air traffic control to ensure safe flight in all weather conditions and efficient managing of all commercial aircraft. Commercial aircraft pilots rely on their onboard navigation systems and automation, conducting flight under the so-called *instrument flight rules* (IFR). IFR enables aircraft to fly under low visibility conditions, and maintain high levels of safety using different onboard navigation systems. On the other hand, general aviation consists for a considerable part of recreational flights, and most of the general aviation utilizes small, cheap, and relatively slow aircraft to conduct flights. These aircraft are usually not equipped with high-tech navigation systems, and are controlled by relying on pilot skills and the principle of see and avoid. Flying without air traffic control and relying on the outside visual information, is flying under the so-called *visual flight rules* (VFR). In VFR flight, the pilot makes use of pressure sensing devices combined with the outside visual information to maintain ground clearance, and to avoid collisions with other aircraft. However, the pilot's visibility is limited by the viewing angles from within the cockpit and weather conditions. Mid-air collisions happen more often in general aviation than in any other branche of aviation.

In general aviation, when flying under VFR the pilot uses outside visual information for obstacle detection, navigation and attitude determination. When weather conditions become sub-optimal during flight, it becomes more difficult to perform these tasks which could be detrimental to the safety of flight. Therefore, VFR flights are more prone to human error compared to IFR flights. In an attempt to increase safety for VFR flights, MetaSensing B.V. in collaboration with Selfly B.V. has developed an on-board Collision Avoidance Radar (CAR) to aid pilots in these tasks. The task of this 10 GHz Frequency Modulated Continuous Wave (FMCW) radar is to detect airborne objects independent of weather conditions, and all around the aircraft.
A master thesis research conducted at the Delft University of Technology (DUT) investigated

the possibility of using this FMCW radar for attitude determination by using it as a Doppler Navigation System (DNS) (Naulais, 2015). The results showed that the CAR could be used for short-term navigation in a situation where sudden changes in weather conditions required instrument navigation. However, the drift becomes larger over time, which rendered the method less useful for long-term navigation.

Currently, guidance systems for low visibility conditions are exclusively used in IFR flights where guidance from Air Traffic Control (ATC) is also present. VFR flights can benefit from a low cost option that assists in low visibility guidance. Radar technology and complex processing have become cheaper and more lightweight over the last decades. It could be possible to use a small, low cost and lightweight radar system such as the CAR for navigation purposes if the accuracy requirements can be met. Besides scanning the area around the aircraft for other airborne objects, the radar detects the ground surrounding the aircraft as well. Detecting the ground could be useful for purposes of navigation and especially navigation during approach and landing procedures. The objective of this thesis is to investigate this possibility for the current CAR.

Literature suggests that a radar technique called synthetic aperture imaging yields high resolution images of the surroundings of an aircraft and is used for example for space missions that focus on mapping the Earth's surface. Synthetic aperture imaging might provide the necessary accuracy in the order of those required for ILS approach procedures. A radar-based navigation system with these properties could add a new dimension to VFR flight where low visibility navigation and landing is possible with regulations that are less strict as those of IFR flight. Also, such a navigation system will operate independently of ground facilities and air traffic control. This keeps the cost and complexity within acceptable bounds while enhancing the possibilities of VFR flight.

Chapter 3

Literature review

The developed CAR could provide assistance in aircraft separation, and possibly in navigation operations in low visibility conditions for VFR flights. Currently, low visibility guidance systems for approach and landing are only available for IFR flights with certified equipment and are only allowed under the supervision of ATC. In order to understand the current state of the art regarding approach and landing procedures the literature on VFR, IFR and airspace classification is revisited (3-1). The objective of this thesis is to understand how radar functionality could support approach and landing procedures in low visibility conditions. For this reason the radar basics are studied and in particular the FMCW radar is discussed. It seems that a synthetic aperture mode of an FMCW radar yields possibilities for high resolution imaging and assistance in approach and landing procedures (3-2).

3-1 Visual and Instrument Flight Rules and automatic landing systems

All airspace is structured using a worldwide airspace classification system, designating areas for specific types of flights and the type of air traffic services that are provided (3-1-1). All aircraft have to follow a specified set of rules depending on the purpose of the flight and the requirements of the flight. Usually all non-commercial flights and other general aviation flights use small lightweight aircraft at low speeds and altitudes, and therefore require little or no guidance from air traffic services. This category can therefore fly according to the so-called Visual Flight Rules (VFR) (3-1-2). Most commercial flights or other flights that require operation under all weather conditions and need guidance from air traffic services to operate safely, fly according to the so-called Instrument Flight Rules (IFR) (3-1-3). Currently, guided landing procedures with automatic systems are used exclusively for IFR flights, and often use the Instrument Landing System (ILS) (3-1-5). Advances were made that could improve accuracy and guidance of the ILS system, by using higher frequency signals. The Microwave Landing System (MLS) has proven to provide all-weather precision guidance for approach and landing. However, during its development, the Global Positioning System (GPS) became available for use for everyone, and provided free guidance using satellites. Since the GPS has been adopted in aeronautics, and can be used worldwide by everyone, several landing procedures have been developed, and are also in use at the time of writing (3-1-6).

3-1-1 Airspace classification

To create order in the airspace, it is subdivided into different regions where air traffic controllers are responsible for the separation of aircraft. The airspace in The Netherlands consists of one Flight Information Region (FIR), the Amsterdam FIR. A FIR consists of controlled and uncontrolled airspace where air traffic control services are responsible for separation. Larger countries may consist of more than one FIR. Within the FIR there are several controlled airspace regions, defined as follows.

- **Control Zone (CTR).** This is a controlled area that stretches vertically from the Earths surface to a defined upper ceiling. In The Netherlands this ceiling is set at 3000 ft. The CTR contains aircraft close to an airport and are guided by a tower (TWR).
- **Terminal Control Area (TMA).** The TMA is used for guidance from airports to air routes and air routes to airports. TMAs are usually defined near busy airports. The TMA is controlled by Approach/Departure (APP/DEP).
- **Control Area (CTA).** The CTA is a larger defined controlled airspace at lower altitudes. In the Amsterdam FIR the CTA ceiling is at FL195. The CTA is controlled by the Area Control Center (ACC).
- **Upper Control Area (UTA).** The UTA is a larger defined controlled airspace at higher altitudes. In the Amsterdam FIR the UTA starts at FL195 and extends upwards. The UTA is controlled by an Upper Area Control Center (UAC). In the Amsterdam FIR this is controlled by the Maastricht Upper Area Control Centre (MUAC) above FL245.

A schematic representation of the airspace region around Amsterdam airport Schiphol is given in Figure 3-1.

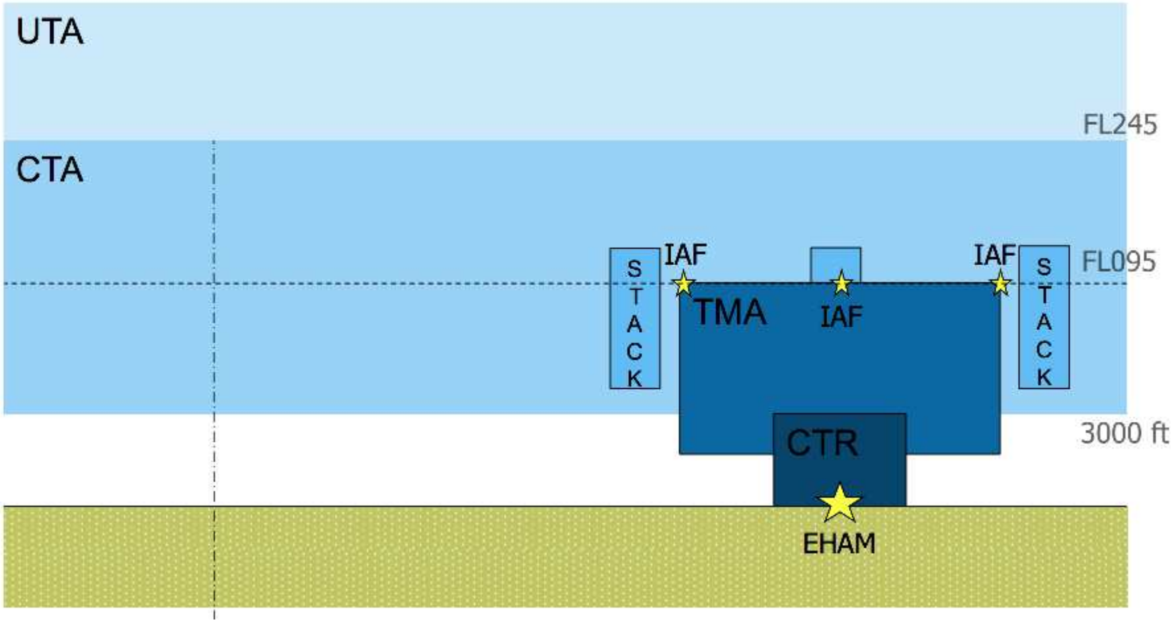

Figure 3-1: Airspace regions around Amsterdam airport Schiphol

In order to regulate and organize air traffic, several airspace classifications have been defined by the International Civil Aviation Organization (ICAO) (International Civil Aviation Organization Annex 11, 2001). Basically, the airspace is divided into controlled and uncontrolled airspace. The airspace classification is as follows.

Class A IFR flights only are permitted, all flights are provided with air traffic control service and are separated from each other.

Class B IFR and VFR flights are permitted, all flights are provided with air traffic control service and are separated from each other.

Class C IFR and VFR flights are permitted, all flights are provided with air traffic control service and IFR flights are separated from other IFR flights and from VFR flights. VFR flights are separated from IFR flights and receive traffic information in respect of other VFR flights.

Class D IFR and VFR flights are permitted and all flights are provided with air traffic control service, IFR flights are separated from other IFR flights and receive traffic information in respect of VFR flights, VFR flights receive traffic information in respect of all other flights.

Class E IFR and VFR flights are permitted, IFR flights are provided with air traffic control service and are separated from other IFR flights. All flights receive traffic information as far as is practical. Class E shall not be used for control zones.

Class F IFR and VFR flights are permitted, all participating IFR flights receive an air traffic advisory service and all flights receive flight information service if requested.

Class G IFR and VFR flights are permitted and receive flight information service if requested.

Under ICAO, the uncontrolled airspaces are Class F and G. All other airspaces are always controlled by air traffic services, but VFR flights are allowed to fly uncontrolled through airspaces D and E as well. The classification of airspaces thus restrict the areas where VFR flight is permitted.
A schematic representation of the airspace classification within the Amsterdam FIR is given in Figure 3-2.

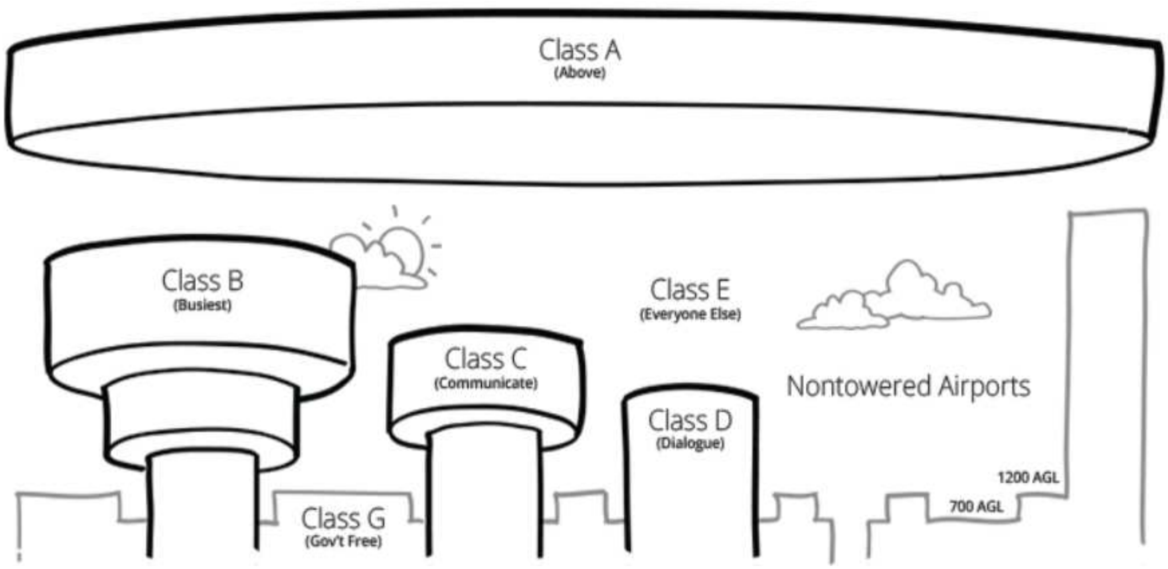

Figure 3-2: Airspace classification in the Dutch airspace

3-1-2 Visual Flight Rules

Visual Flight Rules (VFR) are a set of regulations used for flying relying on the outside visual information, and only using onboard instruments as a reference. VFR requires the pilot to visually detect obstacles, navigate and determine the aircraft attitude. This is important because there is no guidance from air traffic control and because there are no strict performance requirements for the onboard navigation systems. It is not allowed to fly VFR in all parts of the airspace. The airspace is structured and classified to distinguish between busy parts of the airspace around airports and parts that are always controlled by air traffic control, and other areas further from airports. In order to perform VFR flight, the weather conditions must meet the specified minima, summarized in the Visual Meteorological Conditions (VMC), which is specified in the rules of the relevant aviation authority. Also, VFR flights have their own regulations regarding the aerodrome traffic circuits. The next subsections will elaborate on each of these cornerstones of VFR flight.

Visual requirements

Flight rules are laid down internationally and are documented by ICAO (International Civil Aviation Organization Annex 2, 2005). However, some countries require other rules than other countries to ensure safe flight. These differences from the ICAO standards must be

documented in the state's Aeronautical Information Publication (AIP). VFR flight is based on *see and avoid*, where the general rules dictate which aircraft has right of way, and which aircraft should perform what actions when they are on a collision course. A pilot who is required to give way should alter its course to the right, and the one with right of way should maintain heading and speed, but be prepared to take action if the other does not give way. This also requires that VFR flights are conducted between sunrise and sunset.
Internationally an aircraft flying VFR is required to stay 1000 ft above any obstacles in 'congested areas' or any large collection of people, and 500 ft in uncongested areas. The visibility must be such that the flight visibility is at least 8 km. and there are no clouds within 1500 meters horizontally or 1000 ft vertically. At very low altitudes (below 3000 ft Mean Sea Level (MSL)) and in uncontrolled airspace, there are country-dependent exceptions that allow aircraft to fly closer to clouds when they have ground visibility and a speed under 140 knots Indicated Airspeed (IAS) (International Civil Aviation Organization Annex 2, 2005). The VMC minima are summarized in Table 3-1.

Table 3-1: VMC minima as specified by ICAO Annex 2

Altitude band	Airspace class	Flight visibility	Distance from clouds
At and above 3050 m (10000 ft) AMSL	A B C D E F G	8 km	1500 m horizontally 300 m (1000 ft) vertically
Below 3050 m (10000 ft) AMSL and above 900 m (3000 ft) AMSL, or above 300 m (1000 ft) above terrain, whichever is the higher	A B C D E F G	5 km	1500 m horizontally 300 m (1000 ft) vertically
At and below 900 m (3000 ft) AMSL, or 300 m (1000 ft) above terrain, whichever is the higher	A B C D E	5 km	1500 m horizontally 300 m (1000 ft) vertically
	F G	5 km	Clear of cloud and with the surface in sight

Aerodrome traffic circuit

Because general aviation usually fly under VFR, and are therefore not controlled by ATC, flight rules around the runway are defined to keep things orderly and enhance safety. Unless specified differently, all flight circuits are left hand circuits, and of a form similar to that shown in Figure 3-3. The circuit consists of five so-called *legs*, specified as follows and shown in Figure 3-3.

- **Departure leg:** The subsection extending from the runway ahead.
- **Crosswind leg:** The first short side.

- **Downwind leg:** The long side parallel to the runway but flown in the opposite direction.
- **Base leg:** The short side parallel to the crosswind leg flown towards the runway.
- **Final leg:** The subsection from the end of the base leg to the start of the runway.

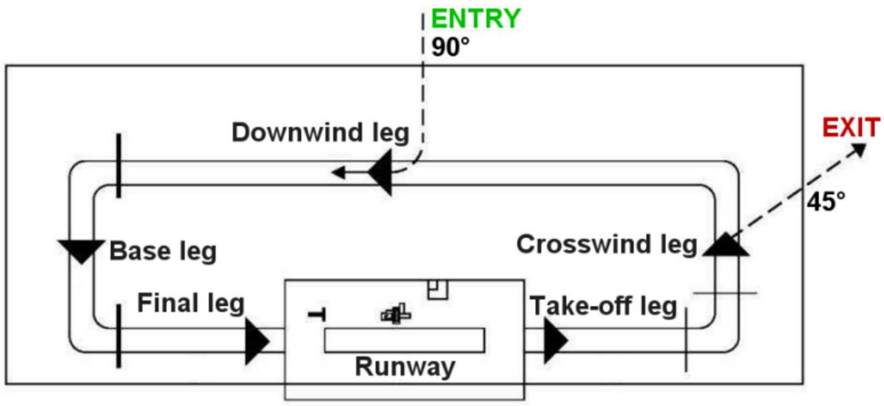

Figure 3-3: VFR circuit defined around a runway

Aircraft flying under VFR that want to leave the circuit should do so on the crosswind leg under a 45 degree angle outwards of the circuit. Aircraft flying under VFR that want to enter the circuit should do so halfway the downwind leg approaching with an angle of 90 degrees in the horizontal plane with respect to the downwind leg.

It is possible to request permission for VFR flight in controlled areas, when the VMC minima are met as specified in Table 3-1. This is known as *special VFR* (SVFR) and is always at the discretion of air traffic control. The ICAO minimum of 1000 ft vertical separation will be applied between IFR and SVFR flights. Between SVFR flights a 500 ft vertical separation will be applied.

3-1-3 Instrument Flight Rules

When flying an aircraft under VFR is not possible, because of the outside visual information being obscured due to e.g. weather conditions, IFR must be used instead. IFR permits flight under Instrument Meteorological Conditions (IMC) which is essentially every weather condition below the VMC requirements, but still safe enough to operate an aircraft. In contrast with VFR flights, IFR flights rely solely on reference using onboard instruments, and navigation by reference of electronic signals. Because IFR flights are always guided by air traffic control services, it is mandatory to submit a flightplan to air traffic control before departure. Moreover, pilots conducting flights under IFR must have a current IFR rating and be trained accordingly.

Instrument requirements

In order to safely conduct IFR flight of a general aviation aircraft, the aircraft should be equipped with a set of basic instruments. The instrument panel can be broken down into three different subsections. The first one is known as the "basic six" and are used to indicate the orientation of the aircraft. These instruments are:

- Airspeed indicator
- Artificial horizon
- Altitude indicator
- Turn and slip indicator
- Directional gyro/horizontal situation indicator
- Rate of climb/descent indicator

Secondly, the pilot uses a set of instruments in order to navigate and to determine the aircraft location with respect to fixed beacons. This consists of at least the following two items:

- **CDI:** Course Deviation Indicator which uses signals from a VHF omnidirectional range beacon or from Instrument Landing System (ILS) equipment
- **ADF:** Automatic Direction Finder which uses non-directional beacons (NDB) for navigation

Finally, there is a set of required systems to monitor the engine status and machinery status and to be able to set the correct parameters for each phase of flight. This set of equipment varies with types of engines and machinery, but includes at least the following items:

- Engine RPM
- Manifold pressure
- Torque setting
- N1 (low pressure turbine) speed
- Engine oil pressure/temperature
- Exhaust gas temperature
- Fuel flow
- Fuel tank quantity

Although many of these instruments are generally also present in general aviation aircraft, the requirements for IFR instruments are more strict in terms of accuracy, reliability and continuity. For this reason IFR instrumentation is significantly more expensive than the instruments found in VFR aircraft.

Approach and departure procedures

An aircraft under IFR has several options to take-off from an airfield. It might do a visual departure if the visibility permits it, or it might get instructions from air traffic control for which heading to take after departure. Also, on busier airfields and more densely populated areas, a so-called Standard Instrument Departure (SID) is used. This is a predetermined take-off procedure that ensures a safe departure from an airfield and causes minimum noise nuisance.
For approach to an airport similar methods are used. The landing of an IFR flight can also be executed visually if the visual meteorological requirements are met, or it can be done using navigation beacons and automatic landing procedures, such as the Instrument Landing System (ILS). Similar to the SID, there is a so-called Standard Terminal Arrival Route (STAR) which is a prescribed landing route unique for each runway to ensure a safe approach with minimum noise nuisance.

3-1-4 Performance-based navigation

Performance Based Navigation (PBN) specifies requirements for aircraft that use onboard equipment to rely on determining their position in terms of their navigation accuracy, integrity, availability, continuity and functionality. PBN helps the structuring of airspace and the efficient navigation of aircraft by ensuring a certain level of navigation performance (Performance-based Navigation (PBN) Manual, 2008). Essentially PBN is propagated through the so-called Area Navigation (RNAV) procedures. Following from RNAV are the requirements of the onboard systems defined in the Required Navigation Performance (RNP) of these systems. Both are shortly elaborated upon in the following paragraphs.

RNAV RNAV is a method of IFR that allows aircraft to use any desired flightpath for navigation, rather than flying from navigation beacon to navigation beacon. This means that the routes are specified in terms of lateral and longitudinal location, rather than radials and distances from ground based navigation aids. This optimizes flight routes and allows for better airspace structuring and therefore greater capacity in any given airspace. RNAV applications are either Basic-RNAV (B-RNAV) or Precision-RNAV (P-RNAV). B-RNAV operations within European airspace require a lateral navigation and along track position fixing accuracy equal to, or better than 2.5NM for 1 standard deviation (68% of the time) and equal to or better than 5NM for two standard deviations (95% of the time). This value includes signal source error, airborne receiver error, display system error and flight technical error. P-RNAV operations within European airspace require a lateral navigation and along track position fixing accuracy equal to, or better than 0.5NM for 1 standard deviation (68% of the time) and equal to or better than 1NM for two standard deviations (95% of the time) (Performance-based Navigation (PBN) Manual, 2008).

RNP RNP systems provide requirements for the performance of onboard navigation aids. Fundamentally it is similar to RNAV, except that it explicitly defines these system requirements in order to ensure system accuracy. There are five types of RNP for general application defined by ICAO. These are RNP 1, RNP 4, RNP 10, RNP 12.6 and RNP 20. In each instance the numerical value indicates the required 95% lateral and longitudinal position accuracy. Detailed specifications of these types of RNP can be found in (Performance-based Navigation (PBN) Manual, 2008).

3-1-5 Instrument Landing System

The ILS is a ground-based navigation system that provides lateral and vertical precision guidance to approaching aircraft for a specific runway. The ILS uses a combination of radio signals and high-intensity light-arrays to enable a safe landing during IMC.
The onboard ILS receivers of an aircraft compare the depth modulations of the received signals. These signals can be routed into the autopilot to fly the aircraft automatically towards the runway guided by the ILS. The ILS works with two independent ground-based subsystems: the localizer for lateral guidance and the glide slope for vertical guidance.

Localizer The Localizer (LOC) is an antenna array usually located beyond the approach end of the runway on both sides. It consists of several pairs of directional antennas. Each side of the runway emits a signal, where one is modulated at 90 Hz, and the other one at 150 Hz. Both these antennas emit a narrow beam of this frequency. If the aircraft receives one of the two frequencies more dominant than the other, it means the aircraft is off-centre with respect to the runway centerline. The needle on the onboard LOC indicator indicates whether the aircraft is too far to the left or to the right of the centerline. The principle is graphically illustrated in Figure 3-4.

Glide slope The Glide Slope (GS) uses a similar technique as the LOC. It is located at one side of the runway at the runway touchdown zone. It modulates two signals on a carrier frequency below and above the approach path. The center of these two lobes is located at a path approximately 3 degrees above the horizontal. When one frequency appears more dominant at the aircraft, the indication is either above or below the glide slope. The principle is graphically illustrated in Figure 3-4.

When the aircraft is locked onto the LOC and GS, the pilot must decide whether to land or not based on the visual reference on the runway near the touchdown moment. The altitude at which the pilot has to decide is referred to as the *decision height*. This decision height is determined by the category of the ILS approach and the equipment of the aircraft and airfield. The different categories for ILS approaches are outlined in Table 3-2.

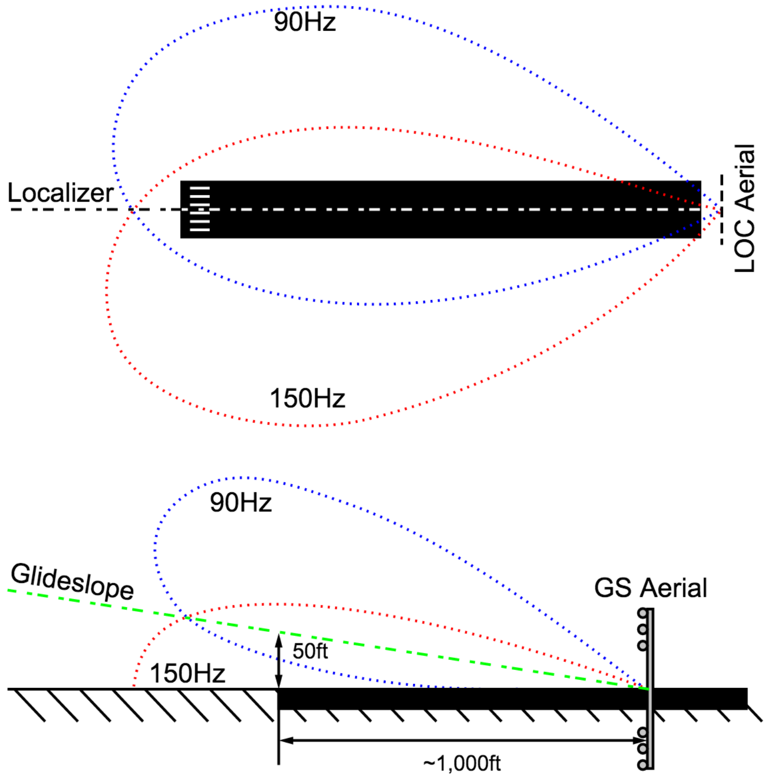

Figure 3-4: Principle of localizer and glide slope frequency emission from the runway

Table 3-2: Available categories for ILS approaches and its requirements

Approach category	**Decision height**	**Runway visual range**	**Visibility minimum**
I	200 ft or more	1800 ft	2600 ft
II	less than 200 ft and more than 100 ft	1200 ft	N/A
IIIa	less than 100 ft and more than 50 ft	600 ft	N/A
IIIb	less than 50 ft	150 ft	N/A
IIIc	No limitations	None	N/A

3-1-6 Modern landing systems

After the ILS system, the Microwave Landing System (MLS) was developed to supplement or replace the ILS system. MLS provided numerous advantages over ILS. MLS has excellent operation in all-weather conditions, it provides more channels to operate on to avoid interference with other systems and a smaller footprint at the airports due to higher frequency operation and therefore smaller antennas. MLS also allows a wide area coverage around the runway, offering approaching aircraft the possibility to choose their approach path from whichever direction they are coming.
However, during its development, it was overshadowed by the advances made with GPS systems. GPS has proven to be more accurate, less expensive to implement and does not require every airfield to upgrade their facilities in order to use it. Because of this GPS advancement, MLS is no longer used and IFR procedures no longer include MLS locations.

GPS offers location and time information of the receiver in all weather conditions and everywhere on Earth using time signals transmitted from satellites. Its implementation has been adopted in aviation in the United States because it lowers the cost for long-range navigation compared to VHF Omnidirectional Range (VOR) and Non-directional Beacon (NDB) beacons (services, 2005). The standard GPS guidance system is not accurate enough to replace ILS for precision-landing procedures. Typical accuracy is around 15 meters, and even for a CAT I ILS approach, the least demanding category, a vertical precision of 4 meters is required (Salih, Zhahir, & Ariff, 2012). A GPS signal can only be received when it is not blocked by any hard surfaces such as buildings. Losing one or more satellite connections on the receiver side cause the position accuracy to be degraded, or yields no position fix at all. However, by broadcasting the correction signal to the GPS receiver, the errors of GPS can be greatly reduced, and this led to the development of Differential GPS (DGPS), which uses separate radio systems to broadcast correction signals to receivers.

Differential GPS Differential GPS provides improved accuracy by broadcasting the correction signal to the receiver, and improves the accuracy from around 15 meters for conventional GPS to centimeter level (Salih et al., 2012). DGPS uses ground-based reference stations, which are at fixed, known positions. By determining these locations using GPS, and comparing these with the known positions of the reference stations, the error correction signal is estimated and used to correct positions of e.g. aircraft that use GPS in the vicinity of that ground-based reference station. The graphical illustration of this system is shown in Figure 3-5 (Salih et al., 2012). The correction signal can then either be broadcasted over short range by the ground station, or from the satellite. Several in depth analyses can be found on the accuracy of GPS by using the properties of GPS signals (L. & L., 2013) (Hwang, McGraw, & Bader, 1999).

In order to increase the level of accuracy and integrity, different augmentation systems are used for GPS-based landing systems which include both Space-Based Augmentation Systems (SBAS) and Ground-Based Augmentation Systems (GBAS). Commonly used are the Wide-Area Augmentation System (WAAS) and the Local-Area Augmentation System (LAAS), both of which are elaborated on in the next paragraphs (El-Rabbany, 2002).

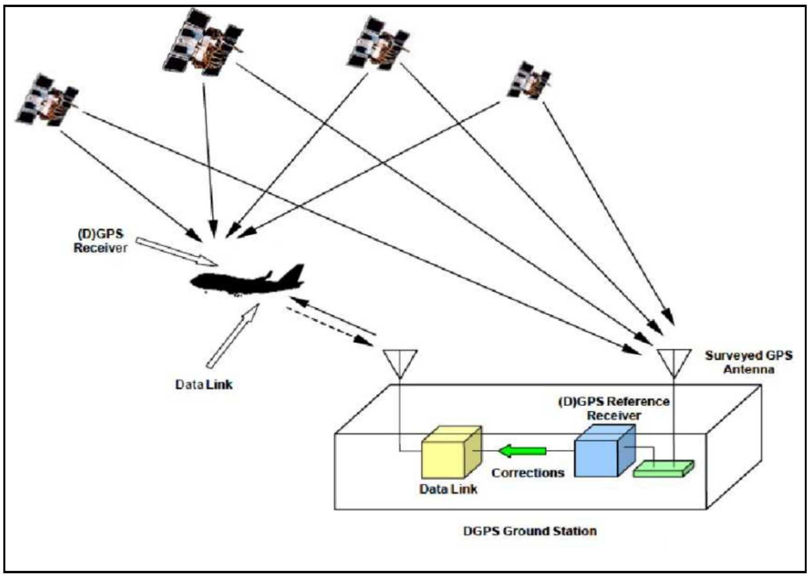

Figure 3-5: DGPS architecture

Wide-Area Augmentation System (WAAS) WAAS is an air navigation aid developed to augment the GPS system in order to improve accuracy and integrity. WAAS enables aircraft equipped with the certified receivers to use GPS for all phases of flight including precision approaches. The WAAS system works by using reference stations, that communicate the local correction signals to a master station. This master station then sends out these correction signals in a timely manner to WAAS geostationary satellites. The WAAS satellites broadcast these error corrections back to Earth, and these corrections can be used by receivers to improve their accuracy. Both lateral and vertical accuracy is specified to be 7.6 meters (25 ft) or better. Actual measurements have shown that the accuracy is better than 1.0 meter laterally and 1.5 meters vertically. These results allow WAAS systems to be used for precision landings comparable to a CAT I ILS approach.

The limitations of this system are caused by the fact that WAAS capable receivers are more expensive than regular GPS receivers, so current receivers have to be upgraded to use this improved accuracy. Also, it will not be able to provide the guidance for a CAT II or CAT III approach. This means that runway requirements in the form of lighting, runway markings and a parallel taxiway are still of effect. Smaller airports which are not ILS equipped should thus still have to upgrade their facilities in order to provide GPS aided approaches.

Local-Area Augmentation Systems (LAAS) The LAAS system is an all-weather system based on real-time GPS correction by using a ground-reference station at a precisely known fixed location in the vicinity of an airport. Its purpose is to provide guidance for precision approaches up to the requirements of the CAT III ILS approach. Local reference stations receive GPS signals and compare the GPS location of the station with the precisely known location of the station to generate a correction signal. This correction signal is then transmitted directly to approaching aircraft using a Very High Frequency (VHF) data link. The aircraft can combine this error correction signal with the received GPS signal to obtain a more accurate estimate of the current position. This information is translated to ILS style navigation aids to provide lateral and vertical guidance towards the runway. Currently, LAAS is only able to provide guidance for a CAT I approach with an accuracy of 16 meters laterally and 4 meters vertically. The limitation of the LAAS system is that it uses RF signals to transmit information, and is therefore jammable. Also, signal degradation due to multipath problems or loss of accuracy due to fading might occur. The principle of LAAS is depicted in Figure 3-6.

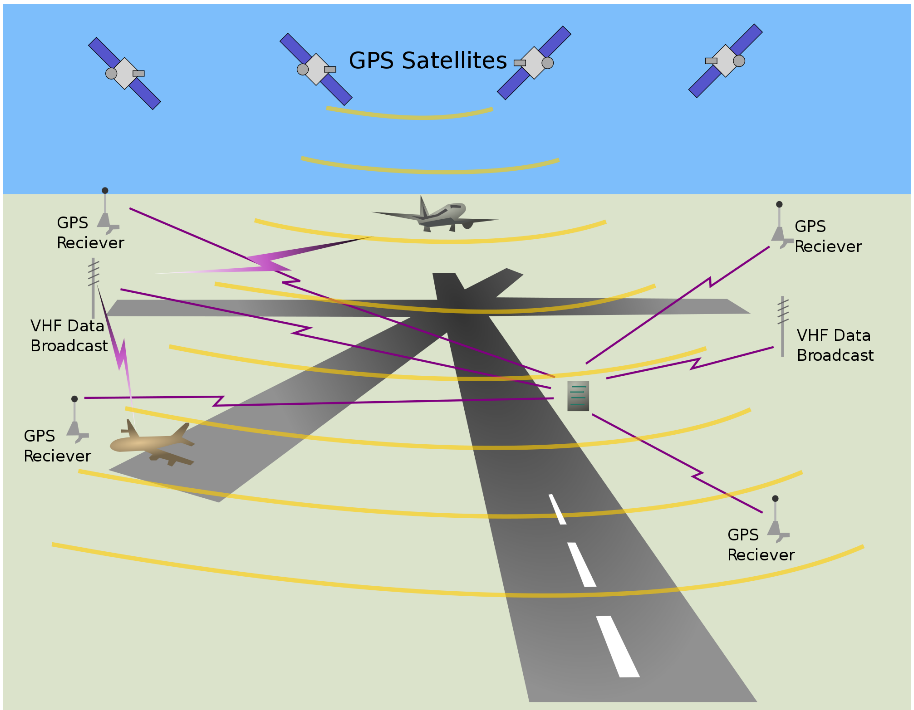

Figure 3-6: Communication streams of the LAAS system

Basic GPS systems are inexpensive and are commonly installed in general aviation aircraft. It seems that GPS systems can also provide the required accuracy to navigate accurately and provide assistance for approach and landing procedures. However, using GPS for this task provides a single point of failure and standard GPS systems do not guarantee the required accuracy at all times. This can be solved by using advanced GPS methods such as WAAS and LAAS, but this increases the cost and dependency on ground facilities in such a way as to render it not feasible for large scale applicability in VFR flights.
The CAR could function as a dissimilar redundancy system for GPS and may provide the required accuracy without increasing cost and without depending on ground facilities. As the CAR already receives echo data about the ground, this might be used for ground mapping using SAR processing algorithms. The next section investigates the properties of radar systems and the possibilities of using the current CAR for navigation purposes.

3-2 Principles of radar

The CAR has been developed to enhance the safety of VFR flight and improve separation between uncontrolled aircraft. The next step is to see whether other facets of VFR flight such as navigation and especially approach and landing procedures can be assisted by the CAR. This section reviews the literature on radar technology and especially FMCW technology which is at the core of the CAR. The possibilities of SAR are investigated as a method to gain accurate information about the ground and airport objects in order to be useful for approach and landing procedures.

3-2-1 Radar technology

A radar operates by radiating electromagnetic waves and detecting the return signal from reflections of the environment. The time required for the electromagnetic wave to return to the radar indicates the distance, or range, between the radar and the detected object. The angular location of a target can be found using a directive antenna, one with a narrow beamwidth, and by detecting the angle of the returning echo. A radar can discern between moving and stationary targets by using the Doppler shift of the echo signal. This allows the radar to find trajectories of moving objects such as aircraft, and make predictions about the future location (Skolnik, 2008). Radar is an active device in that it actively illuminates the target and is not dependent on ambient radiation.

Figure 3-7 shows the principle of a basic radar system and how its components are connected (Skolnik, 2008). The waveform generator usually generates a train of short pulses which are amplified, and sent out by the antenna. The duplexer allows the radar antenna to be used for both the transmission and the reception of signals. Reflective surfaces will reflect a small portion of the transmitted signal back to the antenna and this signal is amplified by the receiver. The raw data can be processed to provide target track information if a target is present and discerned from the surroundings, or the raw data can be analysed for other purposes.

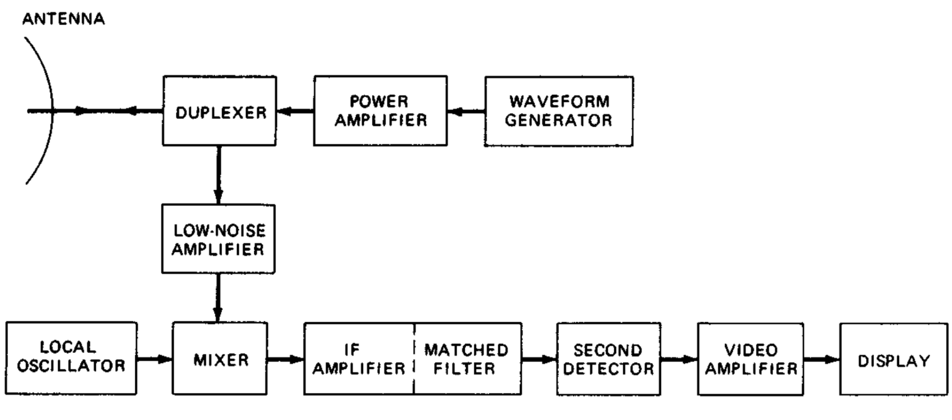

Figure 3-7: Block diagram of a basic radar system employing a superheterodyne receiver

3-2-2 The radar equation

The radar equation gives useful insight into the performance and characteristics of the basic radar as described in section 3-2-1. One form of the equation yields the signal power of the received signal P_r as follows:

$$P_r = \frac{P_t G_t}{4\pi R^2} \cdot \frac{\sigma}{4\pi R^2} \cdot A_e \tag{3-1}$$

The first factor represents the power density of the signal at a distance R meters from the radar antenna. The numerator contains the transmission signal power P_t from an antenna of gain G_t. The denominator accounts for the divergence on the outward path. The second factor numerator is the target cross section σ in square meters, and again the denominator accounts for the divergence, this time of the return path. The first two terms together represent the power per square meter returned to the radar. The antenna of effective aperture area A_e intercepts a portion of this power in an amount given by the product of the three factors. The maximum range R_{max} can be defined when the received power P_r is equal to the minimum detectable signal S_{min}. The radar equation can then be rewritten in terms of maximum range as follows:

$$R_{max}^4 = \frac{P_t G_t A_e \sigma}{(4\pi)^2 S_{min}} \tag{3-2}$$

When a duplexer is employed to use the antenna for both transmission and reception, the transmission gain G_t and effective receiving aperture are A_e are related by $G_t = 4\pi A_e/\lambda^2$, where λ is the wavelength of the radar electromagnetic energy.

3-2-3 Radar echo information

The name 'radar' is derived from radio detection and ranging, but conventional radar systems are more capable then its name implies. A radar usually uses the range and the angle to determine the location of a target. Using the rate of change of these two variables, the velocity and trajectory can be determined.

Range The distance to a target is determined by measuring the time difference of the transmitted signal and the received signal. No other sensor can measure the range at these scales so accurately and under adverse weather conditions as the radar can (Skolnik, 2008). Range is usually determined by using a short pulse as transmission signal. The shorter the pulse, the more accurately the range can be determined. The short pulse has a wide bandwidth. A Continuous Wave (CW) waveform can also be used to determine the range accurately, using frequency or phase modulation. Range measurements with CW waveforms have been widely employed in aeronautics, for radar altimeters and surveying instruments.

Radial velocity The radial velocity can be determined by using the successive range measurements, and determining the rate of change. The Doppler frequency shift of the returning signal is also a measure of rate of change, but it can be unambiguous for pulse radars. When it can be used it is preferred over the rate of change of the range, because it is more accurate and requires less time.

Angular direction The angular direction of the return signal can be measured by using a directive antenna, with a narrow beamwidth. By changing the direction of the antenna to find the strongest signal, the direction of the return signal is determined. This method assumes there is no perturbation by the atmosphere of electromagnetic waves.

Frequency bands Different radar systems operate in different frequency bands, depending on the requirements in terms of accuracy and cost. A summary of the commonly used frequency bands in radar systems is summarized in Table 3-3.

Table 3-3: Frequency bands of radar systems

Band designation	Nominal frequency range
HF	3 MHz - 30 MHz
VHF	30 MHz - 300 MHz
UHF	300 MHz - 1 GHz
L	1 GHz - 2 GHz
S	2 GHz - 4 GHz
C	4 GHz - 8 GHz
X	8 GHz - 12 GHz
K_u	12 GHz - 18 GHz
K	18 GHz - 27 GHz
K_a	27 GHz - 40 GHz
V	40 GHz - 75 GHz
W	75 GHz - 110 GHz
mm	110 GHz - 300 GHz

Frequencies below 300 MHz are used in the oldest radar systems, and are still in use today for long distance ranging. These frequencies follow the curvature of the earth and can therefore be used for over-the-horizon (OTH) communications. Due to the longer wavelength, the physical size of the antenna needs to be large, which reduces the angular resolution of the radar system.

From about 300 MHz up to 1 GHz, radars are used to track long range targets such as missiles and surveillance systems. These systems are also employed for weather systems due to the fact that these frequencies remain relatively unaffected by clouds and rain.
Frequencies from 1 GHz to 2 GHz are mainly used for long-range air-surveillance radars out to about 250 NM. They usually transmit with high power and broad bandwidth.
The S-band uses an even smaller antenna and is used for close ranges up to about 60 NM. S-band radars find their use in some weather systems and airports, where they are used to

track aircraft in the terminal area.

The C-band radar is used for close to medium range targets. The resolution is very high and can be used to track relatively small objects. C-band waves are sensitive to weather conditions which can reduce the useable range even further.

In the X and K_u band the relationship between used wave length and size of the antenna is considerably better than in lower frequency bands. It is widely used in military applications for airborne radars because of their small size and light weight. This frequency band is also very popular for spaceborne or airborne imaging radars based on Synthetic Aperture Radar (SAR) for both military intelligence and civil geographic mapping (Nitti, Bovenga, Chiaradia, Greco, & Pinelli, 2015).

3-2-4 FMCW radar

The Frequency Modulated Continuous Wave Radar is used in the CAR because its relatively low required Root Mean Square (RMS) power resulting in small and lightweight construction. The following sections give in-depth information about the workings of the FMCW radar by explaining the principal workings (3-2-4), followed by the signal processing (3-2-4). The FMCW can also be used for multi-target detection, which increases its application for onboard navigation purposes (3-2-4). Finally, the limitations of the FMCW are discussed to see where it can and cannot be used (3-2-4).

Principle of the FMCW radar

The Frequency Modulated Continuous Wave Radar (FMWC) is commonly used to aid in navigation for aircraft (Skolnik, 2008). Where conventional radars use pulses with separate transmission and reception periods, the CW radar uses a continuous wave where the transmission and the reception occur simultaneously. A normal CW radar is not able to measure distance, because the time delay between transmission and reception can not be measured. By frequency modulating this continuous wave, the form of the wave is known at all instances, hence the delay can be determined. The FMCW radar provides major advantages over pulse radar systems. Since the radar transmits continuously, the transmission power is constant, and therefore is the average power equal to the maximum power. A pulse radar, on the other hand, focusses all its energy on the pulse, and therefore the average power is very low compared to FMCW radars. Since the ability to detect targets is related to the average power, the pulse radar needs to have a much higher maximum power to obtain the same detectability as an FMCW radar. On of the disadvantages of an FMCW radar is the leakage from the transmission signal into the receiver, which limits the maximum usable power of the radar (Undheim, 2012). These radars are primarily used to measure the radial velocity of objects, and the distance between the radar and objects (E. Hyun, Oh, & Lee, 2012).

The FMCW uses a continuous wave that is periodically frequency modulated, with for example a sawtooth waveform with period T, as shown in Figure 3-8. The return echo signal is assumed to be the transmission signal delayed by transmission time τ (Equation 3-3)(Wojtkiewicz, Misiurewicz, Nalecz, Jedrzejewski, & Kulpa, 1997).

$$\tau = \frac{2R}{c} \tag{3-3}$$

Here, R represents the range from the radar to the target and c is the velocity of the microwave. When a sawtooth signal is used, where the frequency increases with time and repeats every time period T (Figure 3-8), the modulation signal can be a sine where the frequency is a function of time (Equation 3-4).

$$x_t = A \sin \Phi_t(t) \tag{3-4}$$

Here, Φ_t represents the phase of the signal, and A the amplitude of the signal. The frequency is the derivative of the phase of the signal (Equation 3-5).

$$f(t) = \frac{1}{2\pi} \frac{d\Phi(t)}{dt} \tag{3-5}$$

As shown in Figure 3-8, the signal increases in frequency over time. The bandwidth of this signal can be mathematically represented as in Equation 3-6.

$$f_t(t) = f_c + \frac{B}{T} t_k \tag{3-6}$$

Where f_t is the frequency of x_t, and t_k represents the time of each period.

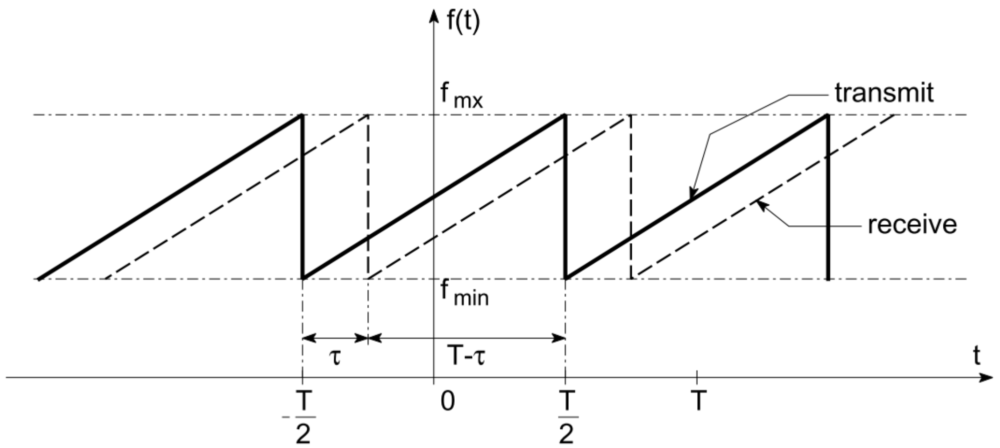

Figure 3-8: Frequency of the transmitted and received signals using a sawtooth waveform

When the signal is echoed back to the receiver, and the target is moving radially with velocity v relative to the receiver, the received signal frequency f_r will have a Doppler shift in the frequency due to the relative motion, and a time shift, due to the distance between radar and target. These two situations are graphically depicted in Figures 3-9a and 3-9b.

Figures 3-9a and 3-9b represent the effect of range and distance on the echo of the transmission signal. When a target has a relative radial velocity with respect to the radar, this

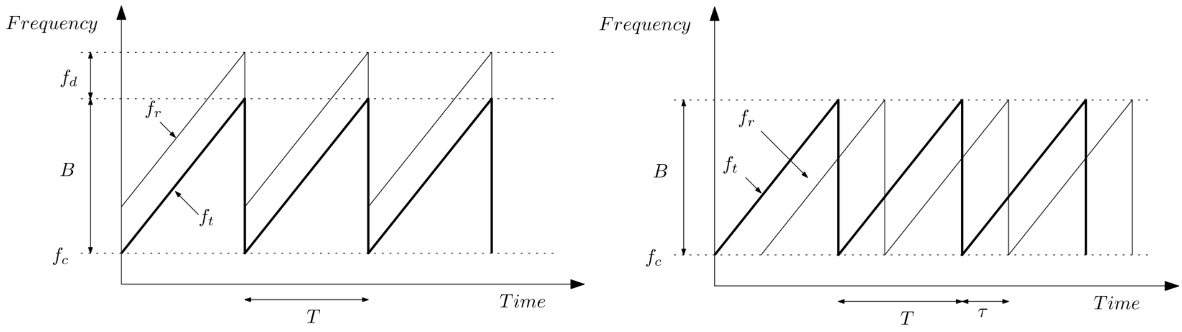

(a) Doppler shift **(b)** Timedelay

Figure 3-9: The difference between the transmitted and received signal due to Doppler shift and timedelay of the echo signal

velocity causes a Doppler shift in the reception f_d (Raney, 1971). The Doppler shift can be mathematically expressed by Equation 3-7.

$$f_d = \frac{2V}{c} f_t \tag{3-7}$$

Equation 3-7 is an approximation, which uses the fact that the velocity of the moving object is much smaller than the speed of light. The Doppler shift is visualized in Figure 3-9a. The distance between the radar and the target causes a time delay in the signal τ. This time delay is mathematically represented by Equation 3-8.

$$\tau = \frac{2s}{c} \tag{3-8}$$

Using both the the Doppler shift of the target and the distance to the radar, the received signal frequency can be described as follows:

$$f_r(t_k) = f_t - \frac{B}{T}\tau + f_d \tag{3-9}$$

Then, the so-called **beat signal** is obtained using mixing of the transmission signal and the reception signal. This beat signal x_b is represented as follows:

$$x_b = A \sin \Phi_b(t) \tag{3-10}$$

With:

$$\Phi_b = \Phi_t - \Phi_r \tag{3-11}$$

Signal processing

The signal processing for the two dimensional case extracting velocity and range, is as described by (Wojtkiewicz et al., 1997). The received signal is combined with the transmitted signal to obtain the beat frequency, as qualitatively described in section 3-2-4. The signal processing is done over K modulations, such that the total integration is KT seconds

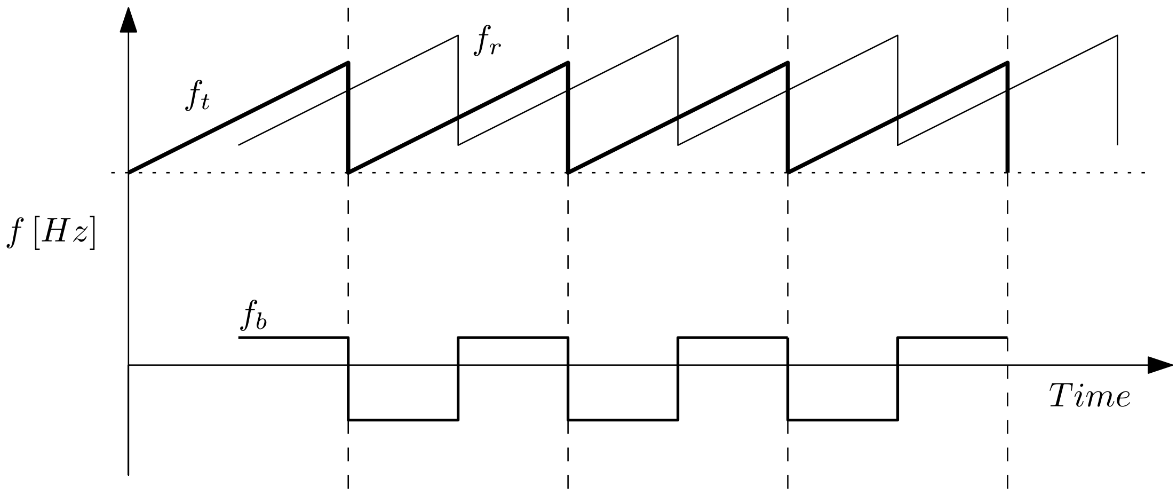

Figure 3-10: The transmission and reception signal (top) and the obtained beat signal (bottom)

(Wojtkiewicz et al., 1997). In this time interval the velocity of the radar is assumed to remain constant and the distance to a single target can be calculated as in Equation 3-12. The transmission signal with reception and beat signal are graphically depicted in Figure 3-10 (Naulais, 2015).

$$s = s_0 + vTk \qquad for \quad k = 0, 1, ..., K-1 \tag{3-12}$$

In Equation 3-12 s represents the distance from radar to target, and s_0 is the distance at $t = 0$.

Rewriting the equation for the time delay (Equation 3-8) the following form emerges:

$$\tau = \tau_0 + \frac{2}{c}(vkT) \tag{3-13}$$

The phase of the beat signal x_b can then be rewritten as:

$$\Phi_b = 2pi\left[\tau_0 f_c + kf_d T + \left(f_d + \frac{B}{T}\tau\right)t_k\right] \tag{3-14}$$

The received signal and the transmitted signal are then combined to create the **video signal** x_v (Wojtkiewicz et al., 1997). This video signal can be 2D Fourier transformed to yield the 2D-profile that represents the range-velocity spectrum of the target. The first Fourier transform is performed on the signal sampled with f_s, with an N-point Discrete Fourier Transform (DFT) for every period T.

$$X_r(\omega, k) = \int_{t_g}^{T} x_b(t)e^{-j\omega t}dt \tag{3-15}$$

This contains the range information of the target. When X_r is treated as a discrete function of k with sampling period T, its spectrum observed in K successive modulation periods yields the following DFT:

$$X(\omega, \theta) = \sum_{k=0}^{K-1} X_r(\omega, k) e^{-j\omega\theta} \tag{3-16}$$

Here, $\theta = \omega_v T$ where ω_v is the velocity frequency. The absolute maximum value of this spectrum yields a value for θ_d, which can be mathematically expressed as $\theta_d = 2\pi f_d T$ where f_d is the Doppler frequency. This Doppler frequency can then be calculated for each corresponding range calculation and this can be graphically depicted in a Velocity-Range (VR) map. The spectrum is periodic in θ, so the result of f_d can only be unambiguously determined within $(-\frac{1}{2T} < f_d < \frac{1}{2T})$. This yields a maximum unambiguously measured velocity of $v_{mx} = \frac{c}{4Tf_0}$.

Multi target detection

Conventional single FMCW radar systems have major issues with multi-target detection, due to the following reasons (E. Hyun et al., 2012):

- separation of ranges and velocities for each target with wide relative velocity
- identification of the correct combinations of beat frequencies of multiple targets is required.

When multiple targets are detected, several up- and down beat frequencies are obtained. The combined processing of these beat frequencies brings out so-called ghost targets, where moving objects are detected that are not actually there, and this degrades radar performance. In order to solve these problems, two methods are generally employed (E. Hyun et al., 2011) (E. H. E. Hyun, Oh, & Lee, 2010) (Winkler, 2007). The first method uses slow ramps with different slopes (Rohling & Moller, 2008) as shown in Figure 3-11. This method has proven to be very effective in accurately determining the range and the velocity of a single target, but still encounters the doppler ghost targets, which require complex algorithms to solve.

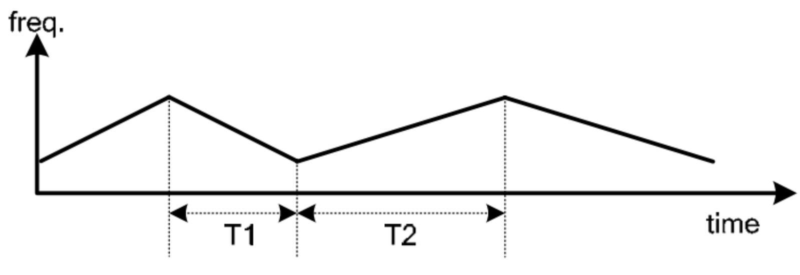

Figure 3-11: Ramp generation with different slopes

The second method is based on fast ramp trains where a 2-step Fast Fourier Transform (FFT) is used to detect the target range and velocity (E. Hyun et al., 2012) as shown in Figure 3-12. Because the movement duration time measurement is very short compared to the target distance, the Doppler shift of the signal is neglected in the first FFT beat frequency. So the range is calculated in the 1st FFT at every Pulse Repetition Interval (PRI) and the Doppler spectrum is calculated at every beat frequency. It has proven to be a very effective method, but computationally very heavy due to the generation of many ramps

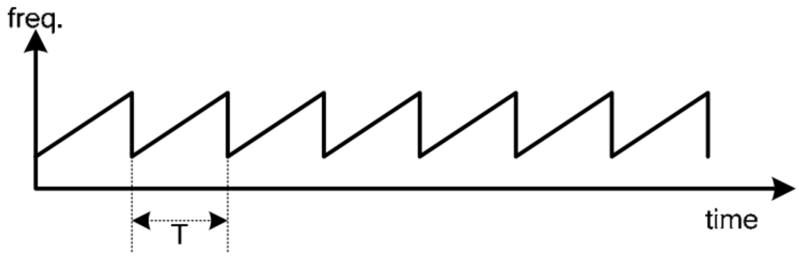

Figure 3-12: Fast ramp generation

(E. Hyun et al., 2012).

In order to find a solution that fits the given problems better, another waveform is proposed that extracts the range and the velocity data in a slightly different manner (E. Hyun et al., 2012). Combining the two methods mentioned before, a two-step waveform is generated as shown in Figure 3-13. The short ramp is used to roughly extract the range in the first period, and the range bound, where the real target exists, is determined using the maximum Doppler shift. In the second period the up- and down- beat frequencies are extracted and the possible combinations for the range-velocity maps are determined. The ghost targets can now be neglected using the range bound found in the first period.

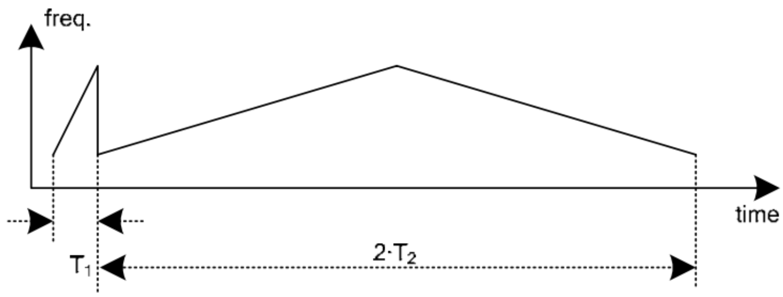

Figure 3-13: Two-step waveform to eliminate ghost targets

Limitations of the FMCW radar

The FMCW radar system is widely used because of the advantages mentioned above. However, there are limitations that constrain the usability of such a radar for specific purposes. According to (Ný, 2009), the limitations are mainly due to systematic errors and random errors, caused by assumptions of linearity and numerical inconveniences. However, (Kulpa, 2001) focusses on the problem of phase noise, being presented as the main issue in FMCW radar systems. The relative importance of the issues depend largely on the application of the radar. Phase noise seems to be the dominant problem when distinguishing moving objects against ground clutter, whereas systematic and random errors appear to pose a challenge in automotive usage, where ground clutter is not the problem, but very accurate measurements of velocity and distance are required. The phase correcting procedure proposed by (Kulpa, 2001) improves the detectability for the simple FMCW radar based on a free-running oscillator. The systematic and random errors can be estimated accurately to provide an indication of the total relative error as formulated mathematically by (Ný, 2009). According to (Wojtkiewicz et al., 1997), the digital signal processing depends on the computational speed and memory storage, both of which have been improved dramatically in the last two decades. The inherent limitations of the radar technique mean that range and resolution have to be compromised in order to find an adequate solution for each application. These are mainly related to the operating frequency of the radar, the details of which are described earlier.

3-2-5 Synthetic Aperture Radar

The FMCW radar can be used in a different configuration to yield high-resolution images of the ground. As explained in the previous sections, finer detail is obtained by using a larger antenna. In order to obtain a high-resolution image of a large area, an antenna array can be used. By having multiple antennas in one array, the gain is increased as each added antenna increases the total transmit power, which yields a higher Signal-to-Noise (SNR) ratio. However, large antenna arrays are impractical for airborne applications because of their size and weight.
In SAR, the aircraft is equipped with a single antenna configuration, continuously sending out signals, that synthesizes an antenna array by virtue of forward movement of the aircraft. The echo of each transmission passes through the receiver and is stored. The Doppler frequency variation for each point on the ground is the unique signature. This is graphically depicted in Figure 3-14 (Chan & Koo, 2008). The SAR imaging system can be used with both a pulsed system or an FMCW system, where the FMCW system benefits from smaller and lightweight equipment.

The geometry of the aircraft mounted SAR is shown in Figure 3-15. The physical aperture of the radar with width W_a and length l generates an RF beam with angular across-track and along-track 3dB beamwidth defined by θ_v and θ_h respectively (Chan & Koo, 2008).
The antenna moves with the flight path vector of the aircraft along the trajectory line with velocity v. It illuminates the shaded area in the figure named the footprint, with the width of the ground swath given by W_g. The forward movement of the aircraft now illuminates the whole swath in the direction of motion of the aircraft.

The benefit of the large synthesized aperture is only available when the antenna looks sideways with respect to the aircraft forward motion. The antenna can not look straight down, because in that situation there is only one range to be measured, which is the altitude of the aircraft. By pointing the antenna sideways as is shown in Figure 3-15, multiple ranges are available and mapping the area is possible.

The SAR radar is able to maintain resolution independent of ground range, when a pulsed radar is used. This happens because the synthesized expanding beamwidth, combined with the increased time a target is within the beam as ground range increases balance each other, such that resolution remains constant. However, FMCW radars can not maintain resolution independent of range. This is due to the nonlinearities in the transmitted chirp signals commonly used for FMCW applications. Several algorithms for processing FMCW SAR signals have been proposed, as described by (Soumekh, 1994). However, this required

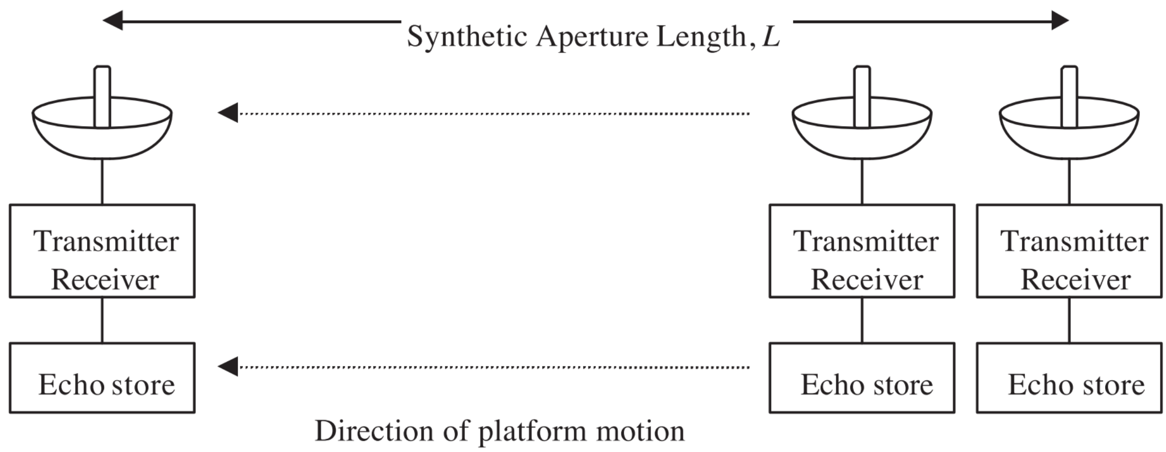

Figure 3-14: Principle of synthesizing a large aperture

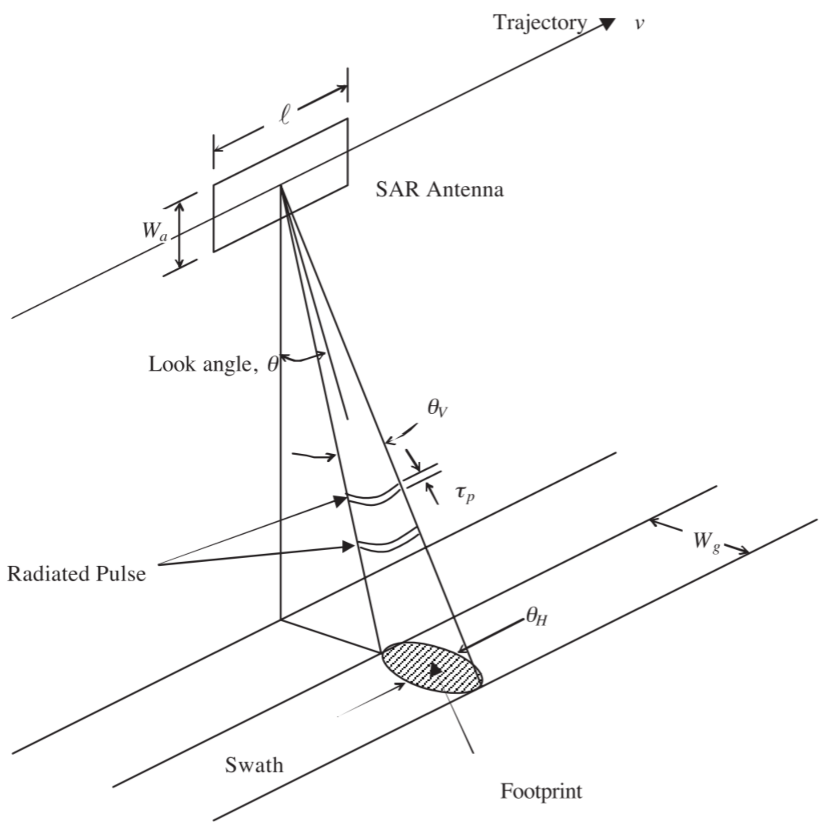

Figure 3-15: Geometry of the imaging of the SAR

the complete bandwidth of the transmitted signal to be sampled and processed by a single Fourier transform over all of the collected data. A different algorithm is proposed by (Meta, Hoogeboom, & Ligthart, 2007) which uses inherent deramp-on-receive operation, and developed algorithms to eliminate the nonlinearity issue. This way, the raw-data bandwidth can be reduced for high resolution systems, which is good because this reduces the size, power and weight of the processing units.

The literature suggests FMCW SAR implementation mainly for imaging areas for geological or weather purposes. Papers describing methods to use SAR for detecting moving targets already go back four decades (Raney, 1971), but very little literature discusses its usability in navigation purposes. A study by (Nitti et al., 2015) investigated the possibility to use a SAR radar as a dissimilar redundancy navigation aid to support Unmanned Aerial Vehicles (UAV) to eliminate drifts on medium-altitude long-endurance flights. In this application the SAR data acquired was correlated with landmarks and could be used when GPS systems failed to aid the Inertial Navigation System (INS) to correct for drift.

Chapter 4

Research questions and set-up

From the literature it seems that VFR is not yet able to ensure high performance in low visibility conditions. Also, the safety of VFR is less established due to the fact that collision avoidance relies on see and avoid, which is prone to human error. General aviation flying under VFR is now limited in capabilities because no reliable on-board systems can ensure safe flight in terms of separation between aircraft and approach and landing procedures. While GPS seems a simple solution for the three facets of VFR flight (navigation, attitude determination and collision avoidance), in order to meet the required accuracy, additional ground facilities are required which render it an expensive operation. Radar technology has become relatively cheap and processing power is more readily available for consumer electronics. The developed CAR provides a low cost, small and light-weight solution for the enhancement of safety by providing collision avoidance assistance. Previous studies have investigated the possibility to perform CAT I approaches using the DGPS facilities with general aviation, but these are still dependent on ground-facilities which renders it only useful at qualified airports (Diana, 2015). A study by (Nitti et al., 2015) has shown that the combination of SAR imaging with a Digital Elevation Map (DEM) can provide position determination, with respect to any object that is included in the DEM. This study used SAR imaging for determining position and IMU drift on endurance UAV flights. In 1994 (Loss, Nicosia, & Taylor, 1994) published a paper that used Autonomous Precision Approach and Landing System (APALS) to describe the possibilities of SAR data combined with GPS and IMU to be able to do precision approaches with general aviation aircraft using the weather radar. This was done using the X-band and with the goal of getting accuracy for CAT III approaches using an accuracy of 1m provided by the radar (Loss et al., 1994).

The literature suggests that no attempt has been made to use radar technology and in particular SAR imaging for enhancing the safety of VFR flight. The CAR provides collision avoidance assistance, and attempt have been made to use it for attitude determination. While the radar seems able to provide attitude determination, the technique relies on dead-reckoning and results in a significant drift over time (Naulais, 2015). The CAR can now be further improved upon by investigating the possibilities for navigation capabilities.

This could be especially useful in approach and landing procedures where high accuracy is required. SAR imaging seems a viable option to meet these accuracy requirements. SAR does provide very high resolution images in either the X-band or Ku-band, but can only be used to look sideways (Raney, 1971). The potential of this functionality is the ability to scan an airfield, runway and its surroundings with very high resolution to check for any obstacles or other approach-inhibiting issues. However, current approach procedures for VFR flights are described in Section 3-1-2, and this relies on visual information on the runway on final leg. This would result in a blind period on the SAR image which could be crucial for landing an aircraft. Using this system in CAT I ILS visual conditions where the cloud base must be 200 ft or higher, the pilot still uses a visual confirmation of the runway and his position before proceeding with the final approach and touchdown.

Essentially this will come down to a form of *Enhanced-VFR* where the strict rules, procedures and ATC guidance of IFR are omitted, but technological advancements are implemented to be able to bring VFR to a higher level of autonomy.

The following sections will elaborate on the research question that emerges from the literature review (4-1), and the accompanying frameworks that function as the foundation for the research proposal (4-2). Finally, the research question is subject to a hypothesis based on the preliminary research results (4-3).

4-1 Research question

From the previous research on the subjects discussed it appears that all individual technologies are well understood and widely used in the aerospace industry. However, very few attempts have been made to combine these technologies for the benefit of precision approaches in general aviation aircraft and airfields without precision approach facilities.
This research proposes to investigate the possibilities of combining these existing technologies toward a specified procedure that allows precision approaches similar to CAT I landing procedures for general aviation aircraft without any dependency on ground facilities at the runway. The collision avoidance radar (CAR) has shown to be a relatively low cost and small radar solution for detecting obstacles and other aircraft. The modifications of this radar to be used in SAR mode could yield positive results for obtaining high resolution information about the aircraft surroundings. This leads to the main research question and is formulated as follows:

Research question: Can the collision avoidance radar be used as a tool to perform unaided approaches under low visibility conditions?

The research question is defined by independent/dependent variable relationships, which is elaborated upon in the following section. Chapter 5 will elaborate on the method that will be used to investigate the relationship between the proposed variables and answer the research question.

4-2 Set-up of the research

The research set-up captures the independent/dependent variable relationships that govern the research question and leads to a methodology to answer the research question. The first part of the research focuses on determining the required accuracy for a radar-based navigation system that leads to safe approach and landing procedures for VFR flights. The required accuracy will be measured at the CAT I condition with a cloud base at 200 ft. Any deviation at this point should be corrected for by the pilot before landing the aircraft.

The second part of the research is concerned with the development of a SAR module that uses the CAR for its source of information. The CAR already provides information about the ground surrounding the aircraft. The SAR module should use this information in such a way as to provide an image of the ground with the required accuracy as specified by the first part of the research. The ground data can be compared to a known object database to obtain a position fix. A radar simulator with the specification of the CAR will be used for the development of the SAR module.

These two parts are captured in separate frameworks where the position accuracy is related to the approach performance, and the landing site configuration is related to the position accuracy of the radar module. The relationships for both requirements are depicted in Figures 4-1a and 4-1b.

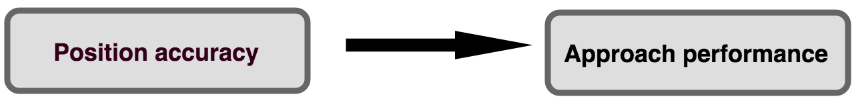

(a) Relationship between the position accuracy (independent variable) with the approach performance (dependent variable)

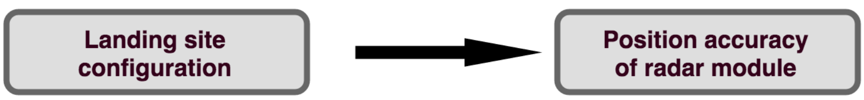

(b) Relationship between the landing site configuration (independent variable) with the position accuracy of the radar module (dependent variable)

Figure 4-1: Relationships of the independent and dependent variables required to answer the main research question of this thesis

In order to delineate the scope of this research, several assumptions are made regarding the independent/dependent variable relationship. The position accuracy of the aircraft is controlled for constant visibility conditions. The visibility conditions are kept constant at the visual range and cloud base equal to a CAT I ILS approach. Other variables during approach and landing are assumed to be equal to the expected values in this phase of flight. It is assumed that current interface design is capable of translating the results of a radar-based navigation system into a form that allows pilots to use it for navigation. Also, the ideal flight

path is assumed to be a constant descent with a 3 degree downward slope up until the runway threshold.
The data processing of the radar is done using a radar simulator developed for project AMOR by Selfly B.V in collaboration with the DUT and MetaSensing B.V. The radar processor is modified in order to investigate its possibilities for being used in synthetic aperture mode, but the underlying assumptions and data sources are retained for the SAR implementation.

4-2-1 Independent variables

In total two independent variables are selected to be controlled, divided over two different parts of research. The first part is the experiment to determine the performance requirements for the navigation module using SAR, second being the development of the navigation module itself using these requirements. The selected independent variables each consist of multiple variables that are directly controllable and measurable. The following paragraphs will summarize the relevance of the independent variable, what it consists of, and how it can be controlled.

Position accuracy The position accuracy is controlled in two dimensions, namely the following:

- Lateral deviation from approach path $[m]$
- Longitudinal deviation from approach path $[m]$

This variable can be controlled by manually giving the approach path guide a deviation of a set value either left or right of the approach path, or below or under the approach path. Given that the controller (pilot) can not verify visually that he is, or is not, aligned with the centerline above the lower cloud base requires him to act upon any deviation when clearing the lower cloud base. The pilot is required to bring back this deviation to zero, and should be able to land the aircraft in a safe manner.

Landing site configuration The SAR implementation of the collision avoidance radar is expected to yield images of the surroundings of the aircraft. The image should give information about the accuracy and resolution of the obtained images. The accuracy of the image is determinant for its usability as a navigation tool. Therefore, the configuration of a possible landing site should be such that it can be detected reliably with the radar, and compared against a known database of objects as to verify the location of the aircraft. The important variables for these objects are its dimension (width, length and height). These variables can be controlled by building a digital elevation model of objects with different dimension, and process the SAR information on these objects to see if the resulting images correspond to the digital elevation model.

4-2-2 Dependent variables

In total two dependent variables as shown in Figure 4-1 are chosen as the variables to be influenced by the independent variables. Both dependent variables also consist of multiple smaller variables that can be measured directly. The first framework leads to performance measures to the approach and landing procedure. The second being the development of a navigation module using SAR, where the dependent variable is the eventual position accuracy yielded by this navigation module, which again consists of predetermined measurable variables. The dependent variables are shortly elaborated upon in the following paragraphs.

Approach performance The approach performance consists of multiple variables which determine the quality of the approach and landing procedure. These variables are summarized as follows:

- Maximum bank angle [°]
- Maximum pitch angle [°]
- Maximum angle of attack [°]

In order to ensure a safe approach and landing procedure, the mentioned variables should not differ significantly from the base condition. The base condition entails the average approach procedure when no deviations from the approach path are induced. The angle of attack should also never approach stall.

Position accuracy of radar module The SAR receiver measurements and technical specifications yield results in terms of identifying objects and accuracy. The navigation module accuracy will depend on the ability to identify the surroundings of the aircraft, and the post-processing of the echo signals. Therefore this is the dependent variable, and will yield results in terms of object dimensions (width, length and height), and image resolution in meters.

4-3 Hypothesis

The hypotheses are based on the variables that are controlled for the two frameworks as described in the previous section. The first framework investigates the relationship between lateral and longitudinal deviation from the ideal approach path and the performance of the landing. The hypothesis are based on the visibility conditions of a CAT I ILS approach where outside visual information is available below the lower cloud base of 200 ft. The hypotheses for the lateral and longitudinal deviations are as follows:

- A lateral deviation of 100 meters or less will allow the pilot to safely guide the aircraft towards touchdown without any significant performance changes compared to a normal approach path.
- A longitudinal deviation of 150 meters overshoot or less will allow the pilot to safely guide the aircraft towards touchdown without any significant performance changes compared to a normal approach path.

The second framework concerns itself with the accuracy of the radar in SAR mode and to what extent objects of the world can be differentiated. The hypothesis concerning the accuracy of the radar is as follows:

- The SAR mode of the radar will yield results in terms of accuracy of less than one meter. With this accuracy, landmarks can be differentiated and compared with database landmarks to provide accurate (<1m) position determination of the aircraft in the vicinity of an airport.

Chapter 5

Method

This section will elaborate on the methods that are used to answer the main research question using the two separate frameworks posed in the previous section. First, the approach procedure design using the VFR traffic circuit is discussed, and the methodology to design several procedures that could be tested to determine a set of navigation requirements for an E-VFR approach procedure. This yields the requirements that the navigation module has to meet in order to support the procedure (5-1). Second, the radar simulator is discussed and explained. The modifications made to the radar simulator and the development of the SAR module is elaborated upon. (5-2).

5-1 Experiment design

In order to answer the first part of the research question participants are invited to take part in a flight simulator experiment (5-1-1). A flight simulator environment is set up for this at the Delft University of Technology (5-1-2). The flight procedure that is used in the simulated environment will be largely based on the current VFR traffic circuit, complemented with guidance representing the navigation module (5-1-3). In this flight experiment the independent variables will be controlled and the dependent variables will be measured, using predefined flight conditions (5-1-4).

5-1-1 Experiment subjects and briefing

A total of twelve participants took part in the flight experiment. They were selected to represent the flying abilities that could be least expected on VFR flights. The subjects were selected from the Delft University of Technology, with differing flight experience ranging from simulator flight only, to sailplane experience and actual licensed VFR pilots with limited experience on the Cessna 172 aircraft.
The participants were informed about the purpose of the experiment via a briefing that was e-mailed and given in hardcopy before the start of the experiment. Each participant was

asked to sign an informed consent form to ensure that the participants were fully aware of the terms and conditions of the experiment, and were also given their own copy.

5-1-2 Simulation environment

Simulator

In order to operationalize the first framework of the previous section, a flight experiment is set up using the commercial off-the-shelf flight simulator X-Plane 10. This flight simulator allows the exporting of flight variables, and manual manipulation of several variables such as lower cloud base and visual range. Also, X-Plane 10 allows the development of plug-ins that can be used to manipulate the simulator environment, tailored to the needs of the user. The flights were conducted using a Cessna 172 type aircraft. This is because it is a widely used aircraft for training, so most of the potential participants are familiar with it. The assumption is that the technical model is well understood and implemented in X-Plane 10. The test environment for this experiment was fixed-base flight simulator. Saitek control units were used for the steering column, throttle pedestal and rudder pedals. X-Plane 10 was displayed on a television screen, with the distance between the participant and the screen ensuring a field of view of 45 degrees, which was also the setting in X-Plane.

As discussed, the SAR limitation is that it can only 'look' sideways, but has the potential to do so with a very high resolution. The downwind leg of VFR traffic circuit provides the ideal condition to scan the airfield and runway with the SAR, and provide the crew with runway obstacles, or moving aircraft on the ground. Depending on altitude and the SAR range, the base leg will still allow the SAR to provide the crew with ground information, but on final leg there is no longer any live information available. This means that the aircraft will be instrumentally blind on final leg, and the pilot must eventually rely on outside visual information to determine whether safe landing is possible, or not. This calls for a decision height and visual range to be determined that allows safe landing. The decision height will be equal to the lower cloud base, since from this point on, the pilot looks outside to see the runway and decide whether to proceed landing or to go around. This will define the required navigation performance that determines how well the navigation module should be able to provide data (Figure 4-1b).

No actual SAR module was used in the experiment, because it has not been developed yet. This experiment mimics the conditions in which the SAR module should be able to yield useful information about the surroundings, in order to land the aircraft safely in low visibility conditions. The goal of the experiment is to yield information about the required accuracy of such a navigation system. Given that the system provides guidance up to the lower cloud base, inaccuracies of a navigation system in terms of lateral and longitudinal deviations are simulated.

Data collection

X-Plane 10 allows the operator to directly export variables from the simulator to a .txt file with a preset frequency. The variables that were exported directly from X-Plane 10 are summarized in Table 5-1. The record frequency of all variables was 5 Hz. This rate was chosen such that no quick state changes could be missed. The assumption is that the Cessna 172 aircraft can not have a significant change of its state within a 0.2 second time period. The live exporting of variables during simulation posed no detrimental effect on simulator performance, as was verified with the frames per second of the simulator. This data is collected for all the experiment conditions, as well as for the familiarization flights, in order to establish a baseline for the results. The part of the data used for analysis starts at the point where the participant descends below the cloud base. This is because in this phase of the flight the participant is required to perform a correcting manoeuvre toward the runway. The behavior of the aircraft during this correcting manoeuvre is compared with the behavior on the familiarization flights in order to see how the variables differ for the experiment conditions with respect to a steady descent.
The simulator data is processed with a custom Python program. The details of this code can be found in Appendix A.
Besides the simulator data, the participants were asked to rate every experiment condition using the Cooper-Harper rating scale (Cooper & Harper, 1969). Using this method, a subjective rating of the handling qualities of the aircraft is obtained for each condition. The Cooper-Harper rating scale was given to the participants beforehand, so that the participants could familiarize themselves with the rating scales. Where the simulator data was automatically extracted in-flight, the Cooper-Harper data was manually noted by the experimenter for each flight condition.
All data was stored anonymously, and can not be used to trace the performance of any individual by name.

Table 5-1: Data variables and units

State variable	Description	Unit
Sim time	Flight time since the simulation was initialized	Seconds $[S]$
IAS	Indicated airspeed	Knots $[KTS]$
G_n load	G load along aircraft Z axis	G-force $[G]$
G_a load	G load along aircraft X axis	G-force $[G]$
G_s load	G load along aircraft Y axis	G-force $[G]$
El yoke	Elevator control input	–
Ail yoke	Aileron control input	–
Rud yoke	Rudder control input	–
M	Pitch moment around c.g.	Newtonmeter $[Nm]$
L	Roll moment around c.g.	Newtonmeter $[Nm]$
N	Yaw moment around c.g.	Newtonmeter $[Nm]$
θ	Pitch angle	Degrees $[°]$
ϕ	Roll angle	Degrees $[°]$
ψ	Heading	Degrees $[°]$
α	Angle of attack	Degrees $[°]$
Altitude	Pressure altitude (MSL)	Feet $[f]$
X	X location in X-Plane coordinates	Meter $[m]$
Y	Y location in X-Plane coordinates	Meter $[m]$
Z	Z location in X-Plane coordinates	Meter $[m]$
Gear1	Force on strut gear 1	Newton $[N]$
Gear2	Force on strut gear 2	Newton $[N]$
Gear3	Force on strut gear 3	Newton $[N]$
C_l	Lift coefficient	–
C_d	Drag coefficient	–

5-1-3 Flight procedure

Several approach situations are designed with different values for the mentioned control variables. In order to simulate this, the standard VFR traffic circuit will be partially flown, starting on downwind leg to fly the complete approach. This method is chosen because from downwind leg on, position accuracy will be increasingly important towards the threshold of the runway. Also, downwind leg would provide the ideal spacial set-up to scan the airfield using a sideways looking SAR. The VFR traffic circuit is shown in Figure 5-1.

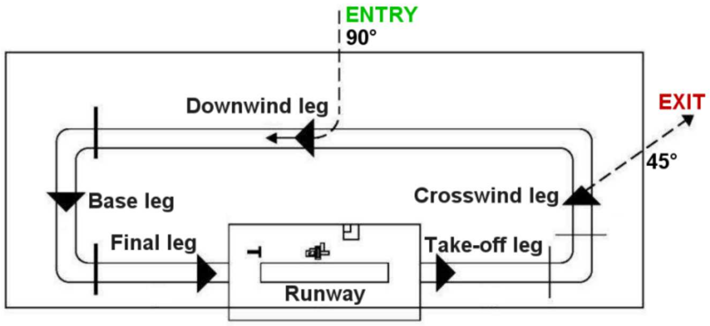

Figure 5-1: VFR circuit defined around a runway

The flight starts by loading a preset location and aircraft state such that the aircraft is looking at the downwind leg at a distance. The flight proceeds by flying towards the downwind leg and making a right turn following downwind leg using the tunnel. The procedure is shown in Figure 5-1 at the 'entry' point.

In order to simulate the guidance from a navigation module using SAR, and the visual translation to a useful interface, a tunnel in the sky is used to guide the aircraft through the VFR traffic circuit without ground visuals. The location of the tunnel is altered to control the lateral and longitudinal deviation of the approach path. The tunnel is created such that the downwind leg height remains constant, as well as the turn onto base leg. From base leg on, a gradual descent with a slope of 3°is maintained until touchdown. A visual representation of the environment is depicted in Figure 5-2. Here, the visibility is set to CAT I conditions, to illustrate the guidance of the tunnel without visual cues from the environment. The opacity of the tunnel is decreased below the cloud base because the subject will use outside visual information for navigation from this point.

5-1-4 Experiment conditions

After the aircraft descends below the preset cloud base, he needs to recover from his lateral and/or vertical error. Examples of both scenarios are shown in Figure 5-3a and Figure 5-3b.

The visibility conditions of a CAT I ILS approach were used throughout the experiment so that the pilot is given the opportunity to verify his location and the runway after the blind period on the final leg. Given these conditions, variations in the lateral and longitudinal offset w.r.t. the ideal touchdown point (pre-defined on the runway and shown to the

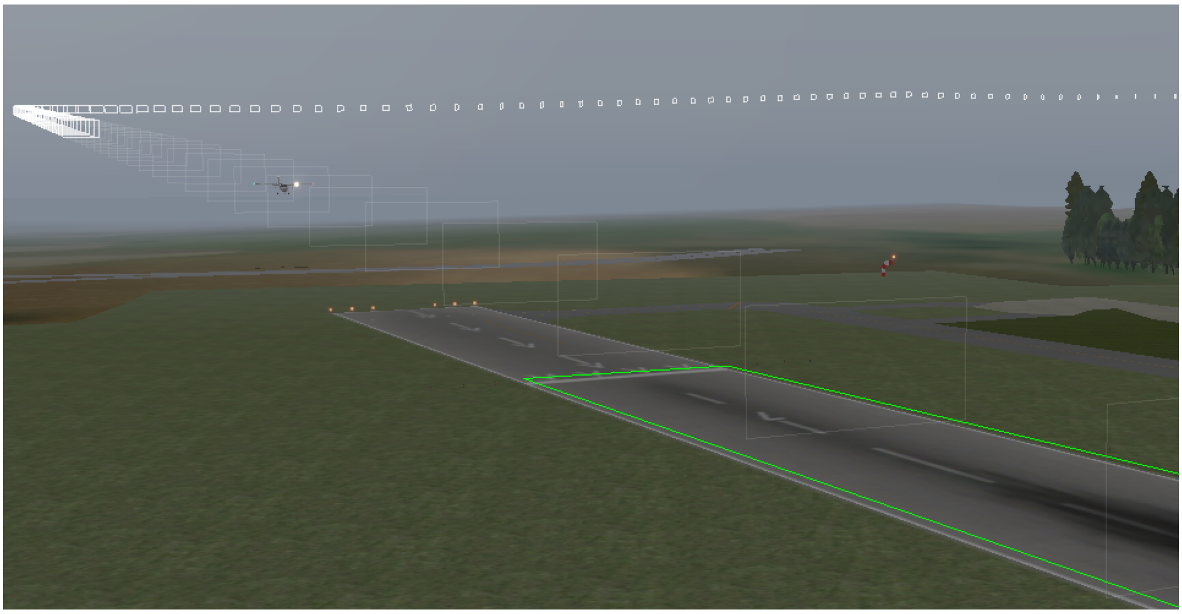

Figure 5-2: Tunnel in the sky implemented in X-Plane to represent the VFR traffic circuit, provided as guidance in low visibility conditions

participant) were introduced to see how well they could be coped with. The limits where a safe approach and landing would still be possible were determined during a pilot-experiment with an experienced VFR pilot, flying multiple approaches. The first approximations showed results of about 100 meters lateral deviation and about 150 meters longitudinal deviation. Using these limitations, twelve conditions were generated around these limits, consisting of lateral deviations, longitudinal deviations and a combination of the two. The cloud base was kept constant at an altitude of 200 ft.

In order to create a 'worst-case scenario' for the results of navigation performance, a crosswind component is added to all scenarios. The crosswind component is 10 kts with 5 kts gust from direction 156°. This translates into crosswind from the right on final leg.
These testing scenarios are randomized in such a way that the learning effect is cancelled out, using a balanced Latin-square to determine the order of scenarios for each participant. The experiment scenarios are summarized in Table 5-2 where the R and L denote if the aircraft is on the left (L) or on the right (R) relative to the runway on final leg. All longitudinal values signify overshoot. The Latin-square is shown in Table 5-3. The L and R are alternating for the conditions, because it was not known beforehand whether manoeuvering with the wind or against the wind would be easier, and because preferences may differ amongst subjects. Because this varies throughout the experiment, it should be treated as a possible confounding factor when analyzing the results.

In order for the participants to get familiar with the setting and the simulator and controls, four familiarization flights were conducted. These flights used similar conditions to the actual experiment in terms of graphical aid (tunnel in the sky) and low visibility conditions, except that the deviations from the runway were absent so that the traffic circuit led the aircraft

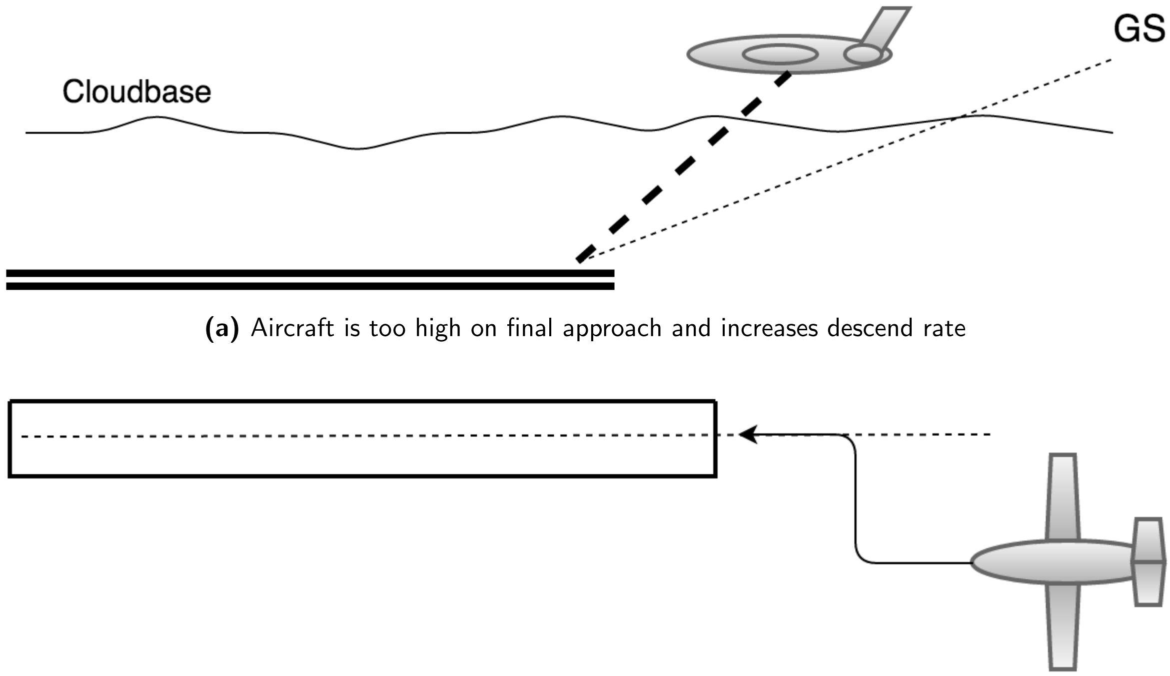

(a) Aircraft is too high on final approach and increases descend rate

(b) Aircraft is not lined up with the runway centerline and needs to manoeuvre to the centerline

Figure 5-3: Graphical representation of longitudinal and lateral deviations from the approach path

straight to the runway threshold. The first two of these four flights were done without any wind component, so that the participant had the opportunity to familiarize with the physical setting and the controls. The second two flights were conducted with the crosswind component, so that the participant had the opportunity to familiarize with wind compensation in the simulator.

Table 5-2: Experiment scenarios with varying lateral and longitudinal deviations from the ideal approach path

	1	**2**	**3**	**4**	**5**	**6**	**7**	**8**	**9**	**10**	**11**	**12**
Lat. deviation $[m]$	200 L	160 R	120 L	100 R	80 L	60 R	40 L	0	60 R	40 L	80 R	120 L
Long. deviation $[m]$	0	0	0	0	0	0	0	300	240 R	180 L	120 R	60 L

Table 5-3: Balanced order of experiments using the Latin-square method

	1	**2**	**3**	**4**	**5**	**6**	**7**	**8**	**9**	**10**	**11**	**12**
Participant 1	1	2	12	3	11	4	10	5	9	6	8	7
Participant 2	2	3	1	4	12	5	11	6	10	7	9	8
Participant 3	3	4	2	5	1	6	12	7	11	8	10	9
Participant 4	4	5	3	6	2	7	1	8	12	9	11	10
Participant 5	5	6	4	7	3	8	2	9	1	10	12	11
Participant 6	6	6	5	8	4	9	3	10	2	11	1	12
Participant 7	7	8	6	9	5	10	4	11	3	12	2	1
Participant 8	8	9	7	10	6	11	5	12	4	1	3	2
Participant 9	9	10	8	11	7	12	6	1	5	2	4	3
Participant 10	10	11	9	12	8	1	7	2	6	3	5	4
Participant 11	11	12	10	1	9	2	8	3	7	4	6	5
Participant 12	12	1	11	2	10	3	9	4	8	5	7	6

5-2 Using the CAR in SAR configuration

A radar simulator has been developed that uses the properties of the CAR to simulate range-rate information on simulated flights in X-Plane 10. This radar simulator formed the basis for this research with respect to the possibilities of using the CAR in synthetic aperture mode. The radar simulator capabilities and limitations are explained in 5-2-1. This simulator is modified such that is supports the CAR in synthetic aperture mode and the model is developed that implements the physics of the synthetic aperture mode (5-2-2).

5-2-1 Radar simulator

Radar specifications

The radar simulator is developed at the Delft University of Technology as part of a PhD research currently carried out by Jerom Maas. The specifications of the radar are not available in this version of the thesis because it is confidential. For more information about the radar specifications, please contact the Delft University of Technology.

The radar antenna emitted power varies with azimuth and elevation angle. This means that the radar emits full power straight ahead, but the signal-to-noise (SNR) drops with increasing azimuth and elevation angle. The radar has a positive value for the SNR between $-38°$ and $+38°$ for both the azimuth and elevation angles. These limits define the window through which the radar is able to receive information. Measurements of this can be found in Appendix B.

Radar systems

The simulator creates a radar system with one transmitting antenna (T_x) and three receiving antennas (R_x). The location of the antennas is defined in the radar system reference frame using and $[X, Y, Z]$ notation. The transmitting antenna has coordinate $[0, 0, 0]$ and the receiving antenna coordinates are defined as the array $[[0, 0, 0.01], [0, 0, -0.01], [0, 0.01, 0]]$. All distances are in meters. A visual representation of this antenna configuration is given in Figure 5-4. The simulator treats the antennas as if they have no size. For clarity they are shown as rectangles in Figure 5-4.

The radar system as a whole is positioned using $[X, Y, Z]$ coordinates with respect to the aircraft body frame. For this experiment they are placed with a 2 meter positive offset on the Y-axis.

Digital elevation model

The radar simulator uses a digital elevation model for obtaining information about the world. The simulator uses data from the NASA Shuttle Radar Topography Mission (SRTM). The results of this mission are publicly available at no cost. The data were sampled at every arc-second, which yields a resolution of around 30 meters, varying with latitude. The files contain a grid of 3601x3601 datapoints. The digital elevation models contain no information about buildings or other artificial elevations.

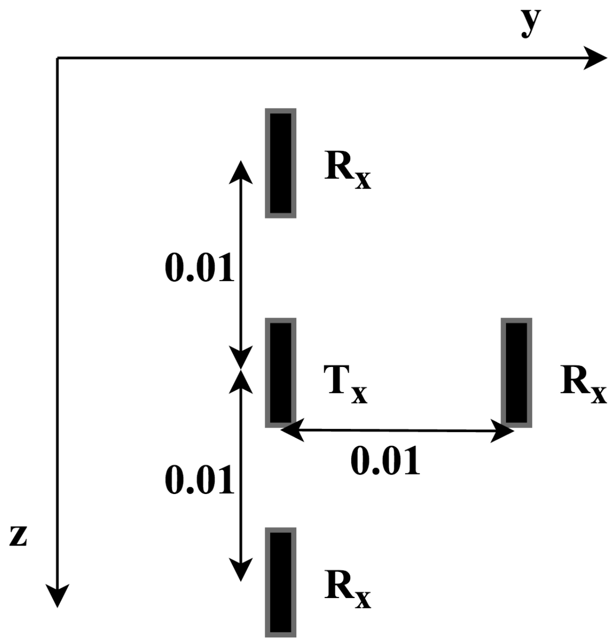

Figure 5-4: Position of the antennas in the radar system

Flight data

The simulator requires an aircraft state in order to determine the position and attitude of the radar systems, as well as the velocity of the radar systems with respect to the digital elevation model. The data required by the simulator and the units are summarized in Table 5-4.

Table 5-4: Required state variables by the radar simulator

State variable	Description	Unit
h_{agl}	Altitude above ground level (AGL)	Meters $[m]$
RoC	Rate of climbing	Meters/second $[m/s]$
v_{gr}	Groundspeed	Meters/second $[m/s]$
ϕ	Roll angle	Radians
θ	Pitch angle	Radians
α	Angle of attack	Radians
β	Drift angle	Radians
ψ	Heading angle	Degrees $[°]$
Lat	Latitude	Degrees north $[°N]$
Lon	Longitude	Degrees east $[°E]$

Radar processor

Given the geometry of the radar antennas, a model of the world and flight data, the radar simulator is able to use this data to obtain results in terms of range and Doppler shift of each point of the DEM relative to the aircraft. The state data is transformed using transformation

matrices to the radar reference frame. The distance between each radar antenna and each point of the DEM is calculated, taking into account the curvature of the Earth. With the same geometric relationships the relative velocity of each point on the DEM w.r.t. the aircraft is calculated.
A simple reflection model is used to determine the amount of power that scatters back to the radar from each point on the DEM. The formula for the reflection of each point on the DEM w.r.t. the aircraft is given by:

$$reflection = sin(\alpha) \tag{5-1}$$

Where α is defined as shown in Figure 5-5. This simple reflectivity model ensures that a far away point with a shallow angle reflects poorly whereas a near point with an angle approaching 90°reflects strongly.

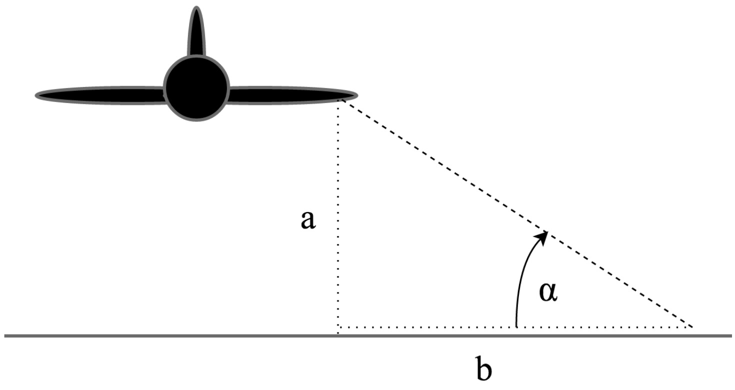

Figure 5-5: Geometry used for the reflectivity model

The reflectivity is required for the radar equation (Equation 3-1). The radar equation gives the power received for each object on the ground. This received power is calculated for each of the receiving antennas. Each antenna reception is in the form of a complex number, with the real part defining the received power, and the imaginary part defining the phase angle of the signal on reception. The different receptions are interfered with each other to get a total of the received power over the antennas and a phase difference between the antennas. The total return signal is then split up into reception power, phase difference, and a vector defining whether or not there was any reception at all.

With predefined axes of range and Doppler shift the data can be used to plot a range-rate map of the surroundings of the aircraft. By default, the CAR is a forward looking radar scanning the ground or other aircraft. While the radar simulator has more modules and can produce more results than discussed so far, this is irrelevant for the current research and is therefore omitted. The values for received power, phase and signal are what is required for the analysis of the implementation of this system as a synthetic aperture radar.

These modules were supplied for this research and remain unchanged. The following section describes the work that was done on the radar simulator in this research in order to obtain results for the CAR in a synthetic aperture mode.

5-2-2 SAR module

The implementation of the synthetic aperture radar requires a modification of the discussed radar simulator. The specifications are not altered for the implementation, because the same physical radar system is used for the synthetic aperture mode. A separate module is created that uses the existing radar processor as its foundation and reconfigures the radar systems. The details of the Python code that was used for the SAR module is explained in Appendix D.

Reconfiguration of the radar system

The radar module is placed an arbitrary distance from the center of gravity of the aircraft using $[X, Y, Z]$ coordinates in the aircraft body frame. For this purpose a dislocation of $[0, 2, 0]$ is used which means the radar module is two meters to the right of the aircraft c.g. (very small GA aircraft, but irrelevant for this purpose). Also, the orientation of the antennas is defined using Euler angles in the aircraft body frame in the form of $[pitch, roll, yaw]$. For this implementation the radar antennas are given a yaw angle of 90 degrees. This means the radar 'looks' in the positive Y-direction of the aircraft body frame. A graphical representation of the radar system orientation is given in Figure 5-6.

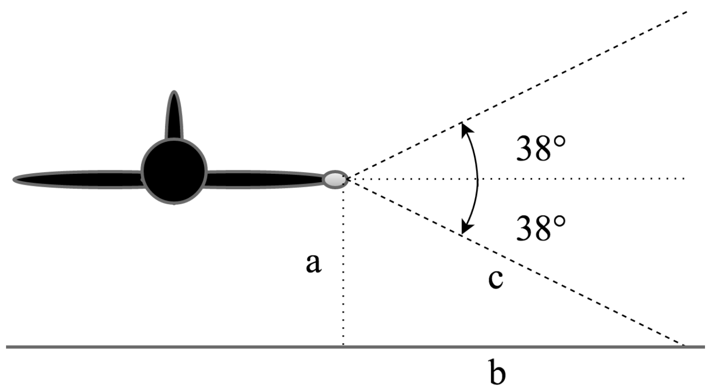

Figure 5-6: Direction of signals in a SAR configuration

Where the angles are fixed because of the radar gain and design, the orientation of the radar system can be altered to look more downwards. The current implementation is to have a pitch angle of $0°$, because this would allow the reception of the radar system to also be used for the collision avoidance radar which looks for other aircraft in the sky. With this orientation there is a limitation as to how close the aircraft can detect ground obstacles. This is defined by the lower $38°$ line in Figure 5-6. The ground distance for the closest object within the radar's view is a function of altitude and is defined as follows:

$$b = \frac{a}{tan(38°)} \tag{5-2}$$

For an aircraft flying in a typical VFR circuit on downwind leg at about 700 ft altitude (210m), this yields a minimum ground distance of $268.8m$. This is the minimum distance from the aircraft at which objects can be detected by the radar for this given altitude.

Physics of the synthetic aperture mode

At the heart of the SAR implementation lies the processing module that uses the raw data of the return signal and transforms it into useful information about the surroundings. The radar processing module as described before remains in use to obtain information about the received power (intensity), phase and reception of each return of the ground. Where the collision avoidance radar checks for each point in the return signal its range and Doppler shift, the SAR uses only the points in the return signal with a Doppler shift of 0. In the case where the aircraft continues in a steady straight symmetric flight, where the direction of movement is along the X-axis of the aircraft body frame, these points with zero Doppler shift are the points in a straight line directly sideways of the aircraft, parallel to the Y-axis of the aircraft body frame. These are the points that neither move closer to nor move further away from the aircraft during transmission and reception of a radar signal. It becomes clear that this last statement must be an assumption, because during the time between transmission and reception the aircraft must have moved. This effect is neglected for velocities that are much lower than the speed of light (the speed of the transmission signal), which is the case for atmospheric aircraft. For example, for a point with a slant range of 3000 meter from the aircraft where the return distance is 6000 meter, the time between transmission and reception with the speed of light ($3e8m/s$) is 0.00002 seconds. An aircraft flying at 85 knots ($43.7m/s$) travels a distance of 0.9 millimeter. When using resolutions that are not in this order of magnitude, the deviation is negligible.
For each point on this line the SAR processor determines the ground distance between this point and the aircraft, and the vertical distance between this point and the aircraft. Doing this for each point yields an array of values that describe the shape of the ground on this line for this instant in time. A graphical representation of the physical geometry is depicted in Figure 5-7.

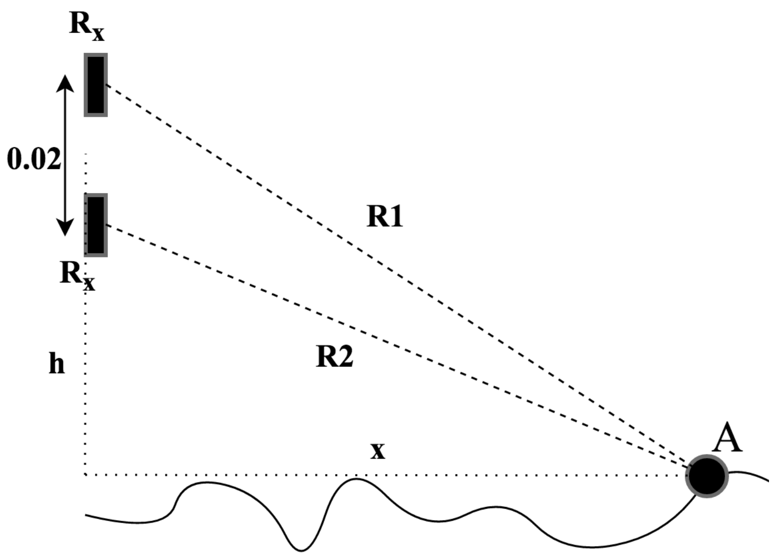

Figure 5-7: Geometric relationships between the receiving antennas and ground points

Here, we see the two vertically aligned R_x antennas receiving an echo of the same point on the ground. The two return signals, R1 and R2, travel different paths towards the receivers.

The return signal is defined by the time it takes to get to the receiver and the phase angle of the sinusoid with respect to the transmitted signal. The distance to the object is calculated with the following equation:

$$R = \frac{c \cdot t}{2} \tag{5-3}$$

Here is c the speed of light and t the time it takes for the signal to travel towards the object and back. Dividing by two is necessary to get the one-way distance. The elevation angle of the object w.r.t. the antenna is calculated using interferometry on the two receiving antennas. A closer look at the geometry of interferometry is provided in Figure 5-8.

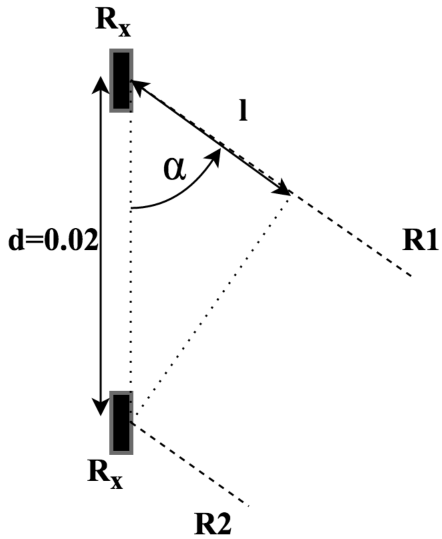

Figure 5-8: Geometry of the interferometry between to receiving antennas

The assumption here is that the signal paths R1 and R2 are parallel. In reality they cannot exactly be parallel because they originate from the same location on the ground and arrive at two antennas separated by a distance d. When considering a slant range $R = 3000m$, and an elevation angle of $\alpha = 90 - 38 = 52$ degrees (maximum elevation angle according to radar gain profile), the difference between R1 and R2 will be $2.5 \cdot 10^{-8}$ meters. With a wavelength of $3.2cm$, this error is many orders of magnitudes lower. For this reason the assumption that R1 and R2 are parallel lines is validated.
Now the distance l defines the difference in the travelled distance between the two reception signals. This difference can be expressed in terms of wavelength λ and phase angle ϕ using the following equation:

$$l = \frac{\lambda \cdot \phi}{2\pi} \tag{5-4}$$

This allows us to write the angle α in terms of l and d as follows:

$$cos(\alpha) = \frac{l}{d} = \frac{\lambda \cdot \phi}{2\pi d} \tag{5-5}$$

It must be noted that for this equation to give unambiguous results, the distance d should never be more than one wavelength λ. For the given situation this condition is satisfied, hence the results are unambiguous. However, in practice the distance between the antennas cannot be 2 centimeters because of the physical size of the antennas. The result is that there are multiple solutions to the equation if ϕ is substituted with $\phi + k2\pi$. To avoid this, either the wavelength should be longer, providing less accurate results, or a mathematical model is required to deal with this ambiguity and find the best fitting solution for the equation. This problem is not considered part of this research and the theoretical model will assume a distance d that is always less than the wavelength λ.

Zooming back out again and looking at Figure 5-7 this expression for $cos(\alpha)$ can be used for the trigonometric relationship between slant range R, vertical distance between aircraft and ground h and horizontal distance between aircraft and groundpoint x. This relationship is mathematically expressed as follows:

$$cos(\alpha) = \frac{\lambda \cdot \phi}{2\pi d} = \frac{h}{R} \tag{5-6}$$

Consequently the ground distance x can be determined using the fact that $x = \sqrt{R^2 - h^2}$. Doing this for each ground point on the line we wish to map, gives an array where each index defines the ground distance w.r.t. the aircraft and a height below the aircraft. This is the desired ground profile result of the SAR. In order to gain sufficient resolution in the range direction, the radar processor is modified such that it analyzes 1000 different ranges between 0 and 5000 meters, yielding a resolution of 5 meters (this resolution is chosen for performance reasons, but in reality the range resolution is only limited by the wavelength of the radar signal). This is done for each consecutive state of the simulated flight and all these arrays are stored to form a grid of coordinates that should describe the ground profile as seen by the radar. Obtaining these states of flight is described in the following paragraph.

Flight data

The radar simulator requires state data as summarized in Table 5-4. It is possible to output these variables in X-Plane 10. A Python program is written and included in the radar simulator that extracts these data columns from the .txt file produced by X-Plane 10 and transforms them such that the right units are used for the radar simulator. This state data is then saved to a .npy file that is read by the radar simulator.
The frequency of the states can be set in X-Plane 10 to any desired frequency. The frequency that is used influences the longitudinal deviation. The used frequencies are mentioned with the results. Information on the state parameters over time for the flight that was used for the SAR model is presented in Appendix E.

Digital elevation models

The radar simulator uses by default digital elevation models from the NASA SRTM. The current models have a resolution of 1 arcsecond and come in patches with a size of 1 degree

latitude and 1 degree longitude. This resolution translates to approximately 30 meters, depending on the latitude. Also, the models do not contain buildings or any other unnatural objects.
As explained, the radar processor will look at 1000 points evenly spaced over the range from 0 to 5000 meters. The echoes are dependent on the properties of the point on the digital elevation model that it reflects. However, when the digital elevation model is defined by discrete points 30 meters apart, and the radar antenna also looks at discrete points within its range, it will only return a signal when these two points exactly intersect. This is not always the case and hence not all points on the DEM are detected. The radar system now has a potential maximum resolution of 5 meters, where the digital elevation model is still 30 meters. In order to obtain a better resolution for the digital elevation model, there are two possibilities. Interpolating the NASA models in order to get a denser datagrid, hence a higher probability of a return signal, or create a new digital elevation model with precisely defined building dimensions and predefined resolution. Both of these options will be investigated and a described shortly.

Interpolating DEM Because the NASA SRTM models are relatively low in resolution for the purposes of this research, the model can be interpolated using a Scipy interp2d function. This function linearly interpolates over a grid of points. The points extracted from the DEM are assigned to arrays of latitude and longitude and evenly spread out. By changing the amount of points in each range of latitude and longitudes, the interp2d function can use a linear interpolation with the points of the DEM to increase the amount of data in the grid. Because the radar looks at a set of discrete ranges, there is the possibility that any given range, there is no DEM point located and this results in an empty echo for that range. Increasing the grid density with interpolation improves the probability that the radar echo contains actual data. The code used for this process is presented in Appendix D. It is possible to interpolate multiple times to increase the grid density further. However, the radar simulator calculates the absolute distance of the aircraft to each point on the digital elevation model. The amount of calculations increases quadratically with the amount of interpolations, causing the simulation time to increase quadratically as well.

Creating a new DEM This option omits a calculation-heavy simulation caused by interpolation, by only creating data where the radar is looking at. With a flight of approximately 8 km this reduces the amounts of calculations by a factor of 100 for any given resolution. Another advantage of this method is that it allows to precisely model the objects in the DEM, which allows for a thorough analysis of the results of the radar compared with what was actually there to see. In order to create a DEM, a separate module is written in Python that creates a large grid of points using Numpy arrays (Appendix D). This model defines a grid of points similar to that in the NASA SRTM model, but does this for a much smaller range of latitude and longitudes. By only defining elevation information in the direct vicinity of the aircraft, the required processing power is reduced and hence higher resolutions are feasible. This model represents a database of objects on a level ground. The default elevation is zero and objects are off-set with respect to the ground. The created model for this experiment is graphically displayed in 5-9.

Six objects have been created on a level map, where the blue background represents an elevation of 0 meters. The buildings range from 5 meters in elevation up to 150 meters in

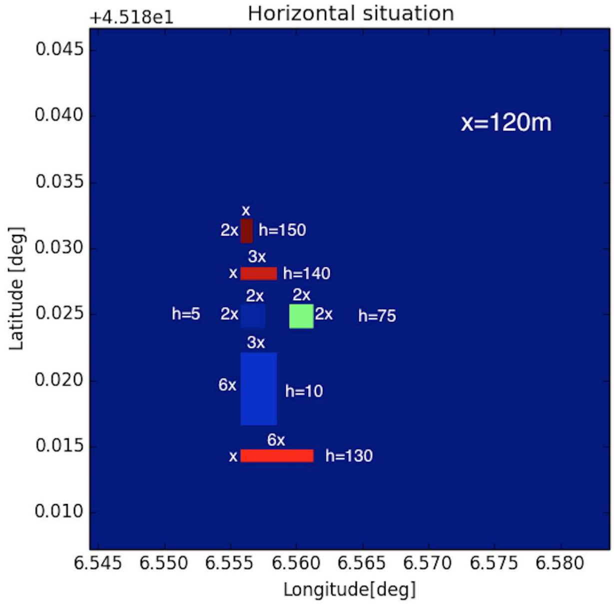

Figure 5-9: The designed geometry of the DEM with the dimensions

elevation. Using this object model on this scale of latitude and longitudes allowed a resolution of 3.59 meters between two points on the DEM.

SAR image stability

The SAR provides an array with range and direction information for each point on the DEM. The geometry of this depends on the attitude of the aircraft. The echo data of the radar is transformed using a transformation matrix to compensate for the aircraft body angles (pitch, roll and yaw). In reality, it is not possible to be sure of the exact state of the aircraft, so noise in these angles might influence the results of the SAR. In order to account for this possible noise, an uncertainty of the aircraft body angles will be introduced to see how this influences the resulting images.

Chapter 6

Results

The results are presented in two different sections to distinguish between the results of the flight experiment and the results of the radar simulator. The results of the flight simulator elaborates on the validation of the data and the appropriate statistical tests in order to present results that reflect the thoughts stated in the hypothesis. The Cooper-Harper rating data is also presented to give the results of the subjective judgments of the experiment conditions (6-1).
The radar simulator is expanded with a SAR module that provides results of the synthetic aperture image based on a DEM. This is done for the NASA SRTM DEM in the Courchevel area, and for a created DEM with predefined objects. In order to verify the stability of the images a stability analysis of the aircraft body angles is presented (6-2).

6-1 Results of the flight simulator experiment

6-1-1 Statistical method and requirements

The experiment is a within-subjects design. Each subject participates in all experiment conditions, and in order to reduce the learning-effect, all conditions are randomized according to the balanced Latin-square method. All the variables collected from the simulator are of the type 'ratio data', because they all have a natural zero point. Because twelve subjects participated in the experiment, there are twelve datasets for each condition and twelve datasets for the familiarization flights.
For the analysis of the data, the extreme values for the variables are considered during the final phase of the flight. This decision is made because the extreme values for the state variables determine whether the flight can be considered safe or unsafe. For example, if the pitch or roll angle assumes at one instant in the flight a value where stall occurs, the manoeuvre should be considered unsafe regardless of the average values for these variables.
Because the data is ratio data, it is considered to be normally distributed in a unimodal way, where the defining features for each variable are its mean and standard deviation. The

statistical test will hence determine whether the data from a given condition and the data from the familiarization flight for each variable are from the same normal distribution. In this case the data is assumed to follow a t-distribution, which is the corrected Z statistic for situation where the mean and standard deviation of the population are unknown, and estimated using samples. The samples are in this case the datasets of the familiarization flights. For this reason the t-test is used as the statistical method with which the datasets are analyzed. Because the experiment is a within-subject design, the appropriate t-test is the paired t-test. Because the paired t-test is a parametric test, the test relies on the following underlying assumptions:

Data fits a normal distribution A normal curve has a skewness of 0 and a kurtosis of 3. Significant deviations from these values indicate that data is not normally distributed. This is tested using the Shapiro-Wilks test.

Data is measured on interval or ratio scale As stated, all the variables from the simulator are classified as ratio data because they all have a natural zero point and describe physical quantities.

Samples are randomly chosen from their populations When selecting the participants, pilots with few experience on either simulator, glider aircraft or powered aircraft were chosen. They are all assumed to represent the least experienced VFR pilots that we could expect in reality.

Equality of variances between distributions Parametric tests can still be robust when the largest variance is not more than 4 times the smallest variance (McKillup, 2006) (Loughin et al., 2006). This is tested for each variable of each dataset against the familiarization dataset.

The results of the equality of variances and normality of the datasets are described and presented in the following section.

6-1-2 Results of the experiment conditions

The statistical results were all obtained with a custom written Python program (Appendix A) that handled the data processing of the raw data from the .txt file. This analysis will focus mainly on the variables *pitch* (θ) , *roll* (ϕ) and *Angle of Attack* (α). This is because these are the directly controlled variables by the subject and most other variables such as moments around the aircraft body axes, rotation rates and control inputs can be derived from these variables. As stated in the previous section, we have to verify that these data sets fit a normal distribution, and that their equality of variance is within acceptable bounds. The distribution of the gathered data for all other variables are shown in Appendix C.

Normality test

The test for normality is done using the Shapiro-Wilk method (Shapiro & Wilk, 1965). This method tests the null-hypothesis that a given dataset is normally distributed. The results

Table 6-1: Results of the Shapiro-Wilk test for normality

	Lat. dev.	Lon. dev.	ϕ $[W, p]$	θ $[W, p]$	α $[W, p]$
Base	0	0	[0.9171, 0.2630]	[0.8955, 0.1386]	[0.9609, 0.7961]
C1	200L	0	[0.9301, 0.3816]	[0.9177, 0.2676]	[0.9384, 0.4777]
C2	160R	0	[0.9142, 0.2414]	[0.6776, 0.0005]	[0.6839, 0.0006]
C3	120L	0	[0.9156, 0.2515]	[0.6524, 0.0003]	[0.6662, 0.0004]
C4	100R	0	[0.9326, 0.4086]	[0.9316, 0.3974]	[0.9046, 0.1819]
C5	80L	0	[0.9520, 0.6669]	[0.9591, 0.7703]	[0.9004, 0.1606]
C6	60R	0	[0.9251, 0.3313]	[0.9566, 0.7346]	[0.5352, 3.251e-05]
C7	40L	0	[0.8999, 0.1581]	[0.7674, 0.0041]	[0.8920, 0.1251]
C8	0	300	[0.8816, 0.0918]	[0.9518, 0.6631]	[0.8866, 0.1066]
C9	60R	240	[0.9642, 0.8417]	[0.8403, 0.0279]	[0.8405, 0.0281]
C10	40L	180	[0.9388, 0.4823]	[0.9408, 0.5086]	[0.8443, 0.0312]
C11	80R	120	[0.9458, 0.5771]	[0.8106, 0.0124]	[0.7840, 0.0062]
C12	120L	60	[0.9245, 0.3252]	[0.9152, 0.2483]	[0.9445, 0.5591]

of the test statistic W and the corresponding p-value are summarized in Table 6-1. Using a 95% confidence interval, p-values larger than 0.05 indicate that the dataset *is* normally distributed.

The results in Table 6-1 show that the variable ϕ passes the test for normality on all conditions. The variables θ and α fail to pass the test for normality on multiple conditions. The normality of the data is improved by performing data transformations. A reciprocal transformation is used for the variables θ and α. The reciprocal transformation transforms $x \rightarrow 1/x$. The results of the Shapiro-Wilk test after this transformation is shown in Table 6-2.

Table 6-2: Results of the Shapiro-Wilk test for normality after transforming θ and α

	Lat. dev.	Lon. dev.	ϕ $[W, p]$	θ $[W, p]$	α $[W, p]$
Base	0	0	[0.9171, 0.2630]	[0.9438, 0.5482]	[0.8006, 0.0010]
C1	200L	0	[0.9301, 0.3816]	[0.9575, 0.7477]	[0.9040, 0.1784]
C2	160R	0	[0.9142, 0.2414]	[0.8990, 0.1541]	[0.9357, 0.4439]
C3	120L	0	[0.9156, 0.2515]	[0.8825, 0.0943]	[0.8951, 0.1373]
C4	100R	0	[0.9326, 0.4086]	[0.9601, 0.7856]	[0.9273, 0.3528]
C5	80L	0	[0.9520, 0.6669]	[0.9536, 0.6898]	[0.9567, 0.7353]
C6	60R	0	[0.9251, 0.3313]	[0.9263, 0.3426]	[0.9123, 0.2285]
C7	40L	0	[0.8999, 0.1581]	[0.8638, 0.0546]	[0.8999, 0.1583]
C8	0	300	[0.8816, 0.0918]	[0.9709, 0.9195]	[0.9800, 0.9838]
C9	60R	240	[0.9642, 0.8417]	[0.9526, 0.6754]	[0.9795, 0.9816]
C10	40L	180	[0.9388, 0.4823]	[0.9606, 0.7923]	[0.9339, 0.4228]
C11	80R	120	[0.9458, 0.5771]	[0.9056, 0.1876]	[0.9357, 0.4445]
C12	120L	60	[0.9245, 0.3252]	[0.9537, 0.6917]	[0.9566, 0.7339]

After the transformation, the p-values for θ are all > 0.05, and for α the base condition does still not pass the test for normality.

Equality of variances

Secondly, the data is tested for equality of variances, or homoscedasticity. This is done using Levene's test for equality of variances. This tests the null hypothesis that all input samples are from populations with equal variances (Olkin, 1960). This test is an alternative to Bartlett's test in the case where there are deviations from normality, as is the case with the base condition for α. The test statistic is calculated for each condition paired with its corresponding base condition, in order to see if the variance from a given test condition differs significantly from the variance of the base condition, so there are twelve tests per variable. The results for the test statistic W and p-value of the transformed datasets are shown in Table 6-3.

Table 6-3: Results of Levene's test for homoscedasticity

	Lat. dev.	Lon. dev.	ϕ $[W, p]$	θ $[W, p]$	α $[W, p]$
C1	0	0	[2.387, 0.1366]	[0.3304, 0.5712]	[0.0636, 0.8033]
C2	200L	0	[2.705, 0.1142]	[0.4347, 0.5165]	[0.8745, 0.3599]
C3	160R	0	[2.599, 0.1212]	[0.4453, 0.5115]	[0.1639, 0.6895]
C4	120L	0	[2.830, 0.1066]	[2.257, 0.1472]	[1.877, 0.1845]
C5	80L	0	[0.5652, 0.4602]	[2.076, 0.1637]	[1.737, 0.2011]
C6	60R	0	[0.9543, 0.3393]	[0.6535, 0.4275]	[3.112, 0.0916]
C7	40L	0	[0.1202, 0.7321]	[0.2989, 0.5901]	[0.5031, 0.4856]
C8	0	300	[0.0007, 0.9791]	[4.923, 0.0371]	[2.2230, 0.1502]
C9	60R	240	[1.335, 0.2603]	[0.5950, 0.4487]	[0.9123, 0.3499]
C10	40L	180	[0.0521, 0.8216]	[0.3504, 0.5599]	[0.8146, 0.3765]
C11	80R	120	[6.127, 0.0215]	[0.4202, 0.5236]	[1.299, 0.2667]
C12	120L	60	[0.3103, 0.5831]	[2.536, 0.1255]	[2.168, 0.1551]

Most conditions pass Levene's test for homoscedasticity, but there are a few exceptions. The roll angle ϕ fails the test for condition 11 with a p-value of 0.0215 which is below the threshold of 0.05. The pitch angle θ fails the test for condition 8 with a p-value of 0.0371.

T-test

Because the tests on normality of the data and equality of variance are in most cases not severely violated, a parametric test will be used to test for significant results between the test conditions and the base condition. The t-test is the appropriate test for significance given the form of the data.
The t-test will test the null hypothesis that two given dataset are from the same normally distributed population. The p-value is again set at the threshold of 0.05. The normal distributions are depicted using boxplots (Figures 6-1, 6-2, 6-3). Note that the untransformed datasets are used, in order to preserve the meaning of the physical quantities. The table on the X-axis shows the lateral and longitudinal deviation for each condition. The notations

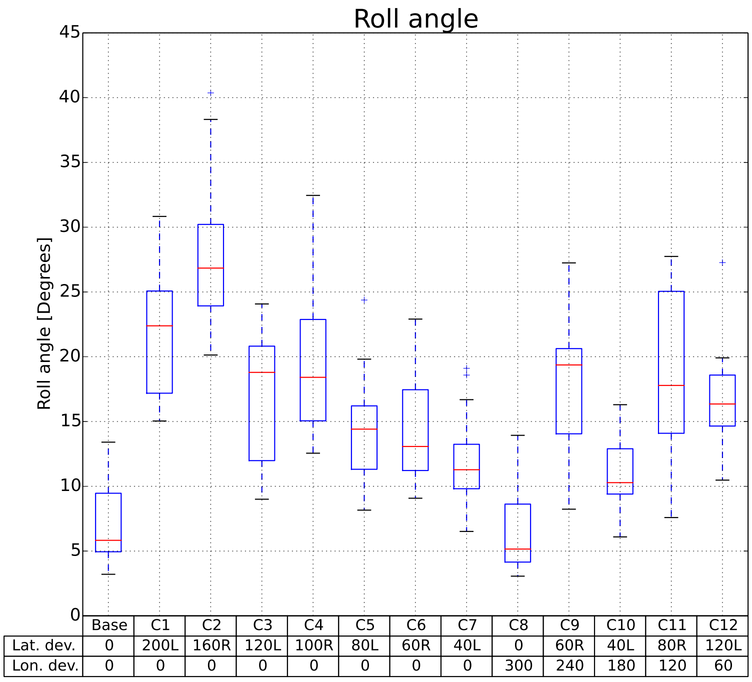

Figure 6-1: Normal distributions of roll angle for all conditions

'R' and 'L' mean right or left of the runway respectively. All longitudinal deviations were overshoot. The results of the t-test on the transformed datasets are shown in Table 6-4.

All values below the threshold p-value of 0.05 mean that the null hypothesis for the given condition and variable can be rejected. If one of the variables for a given condition implies a rejection of the null hypothesis, the approach procedure deviates significantly from the base condition on that variable. Hence, for all conditions the null hypothesis is rejected.

Restating the hypothesis from Section 4-3:

- A lateral deviation of 100 meters or less will allow the pilot to safely guide the aircraft towards touchdown without any significant performance changes compared to a normal approach path.
- A longitudinal deviation of 150 meters overshoot or less will allow the pilot to safely guide the aircraft towards touchdown without any significant performance changes compared to a normal approach path.

Based on the results, it seems that not one condition retains the null hypothesis. This means that each condition can be said to have significantly different distribution of values for these variables than the base condition. This means that both hypotheses as stated above are rejected. While the other variables have been analyzed, they are not presented here because for any one condition to retain the null hypothesis, it should be retained for all variables.

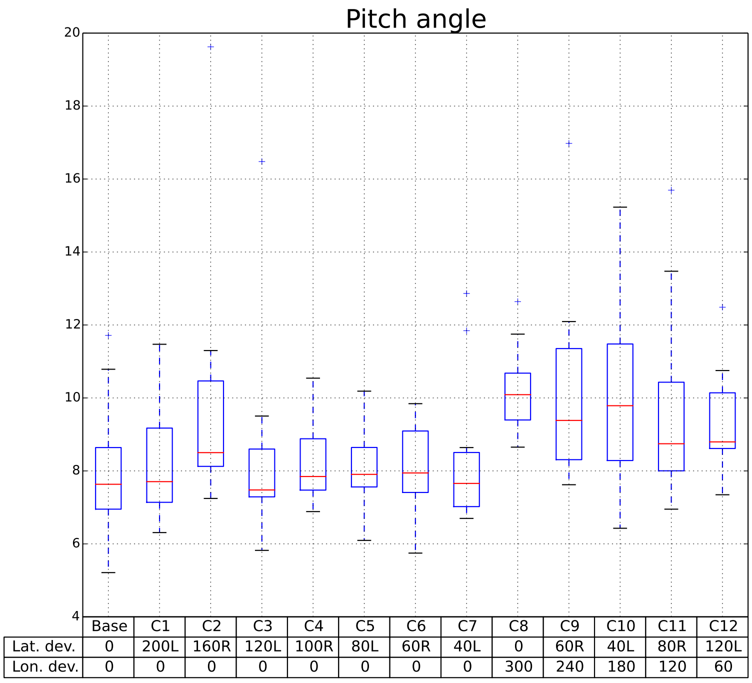

Figure 6-2: Normal distributions of pitch angle for all conditions

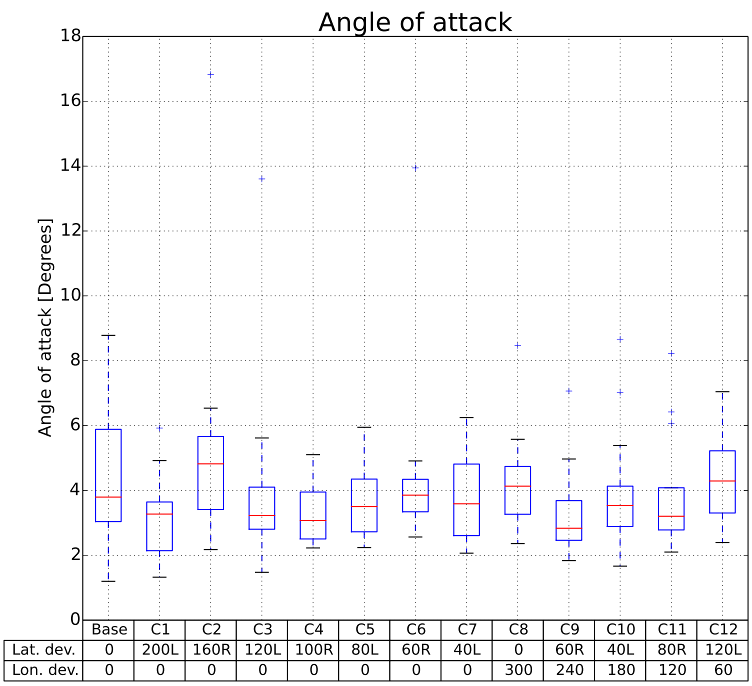

Figure 6-3: Normal distributions of angle of attack for all conditions

Table 6-4: Results of the t-test for ϕ, θ and α for all conditions

	Lat. dev.	Lon. dev.	ϕ	θ	α
C1	200L	0	1.643e-5	0.5838	0.3683
C2	160R	0	1.881e-7	0.0934	0.3762
C3	120L	0	4.230e-5	0.6617	0.7881
C4	100R	0	1.372e-5	0.3058	0.8684
C5	80L	0	0.0011	0.4873	0.8271
C6	60R	0	0.0005	0.6057	0.4059
C7	40L	0	0.0019	0.5882	0.8957
C8	0	300	0.5893	0.0024	0.4601
C9	60R	240	7.910e-5	0.0393	0.6223
C10	40L	180	0.0092	0.0232	0.8840
C11	80R	120	0.0002	0.0630	0.9514
C12	120L	60	0.0001	0.0476	0.3186

6-1-3 Results of the Cooper-Harper ratings

Next to the objective simulator performance data, the subjects were asked to rate each condition using the Cooper-Harper rating scale. This rating scale from 1 to 10 gives the subject the opportunity to provide information about the controllability of the situation. On this scale, 1 is perfectly controllable without any improvements warranted, 10 is uncontrollable and mandates improvement. The subjects were asked if they thought the given situation was acceptable for an approach and landing procedure, or if it required improvements in order to land safely. Ratings 1-3 state that the situation is satisfactory without improvement, ratings 4-6 state that deficiencies warrant improvement, ratings 7-9 state that deficiencies require improvement and rating 10 states that improvement is mandatory. The ratings are presented for each condition, giving a minimum, a maximum and an average Cooper-Harper rating (Table 6-5).

Table 6-5: Cooper-Harper results of each condition

	C1	C2	C3	C4	C5	C6	C7	C8	C9	C10	C11	C12
Lat. dev.	200L	160R	120L	100R	80L	60R	40L	0	60R	40L	80R	120L
Lon. dev.	0	0	0	0	0	0	0	300	240	180	120	60
Minimum	2	4	3	3	2	2	2	2	3	2	2	3
Maximum	9	8	5	6	5	6	5	6	6	5	5	7
Average	5.5	5.4	4.3	4.4	3.8	3.3	3	3.3	4.3	3.5	3.8	5

6-2 Results of the CAR in SAR mode

The results of the CAR in SAR mode are presented using two different digital elevation models as explained in Section 5-2-2. The digital elevation model of the area of Courchevel from the NASA SRTM mission is used (45°N 6°E to 46°N 7°E). Also, a self created DEM is used, the details of which are described in this section. One of the assumptions is that the state of the aircraft is exactly known, so that the geometry between the radar antennas and ground is exactly known. This assumption cannot be met in real life due to inaccuracies of state measurement. A stability analysis is conducted for the body angles where noise in pitch, roll and yaw are induced and their influence on the results is displayed.

6-2-1 Results of SAR over Courchevel area

The flights over Courchevel area are manually flown in X-Plane 10 and a state output frequency of 2Hz was used to log the data. The aircraft was a Cessna-172. The NASA SRTM DEM of this area has a 1 arcsecond resolution, which is equal to 20.84 meters between any two points. The radar range resolution is set at 5 meters, which means that the radar looks for a return echo for every 5 meters of range between 0 and 5000 meters. Because of these discrete datasets for both the DEM and the radar range values, there are gaps in the data where there is no DEM point detected on a given radar range. To compensate for the lack of reception at these points, the echo data is interpolated for the image.
One result of a flight over the Courchevel area and the resulting SAR image is shown in Figure 6-4

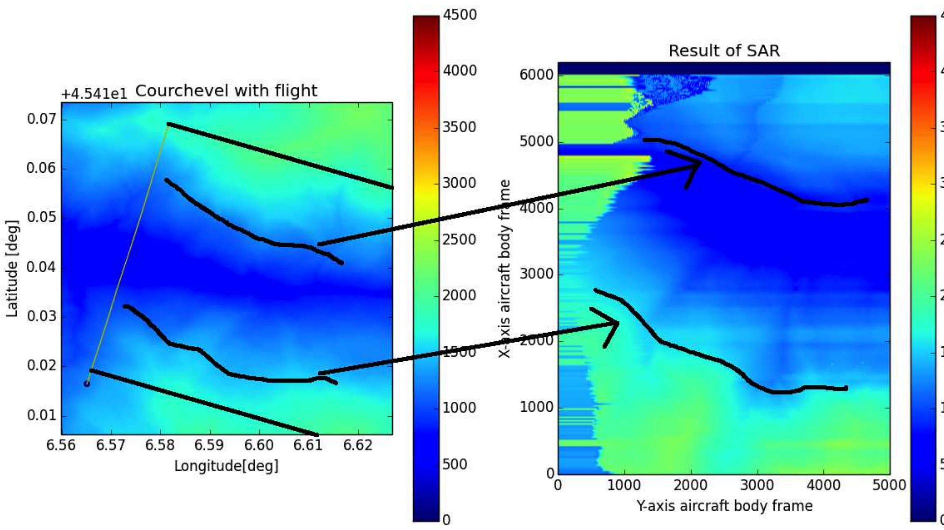

Figure 6-4: DEM of a part of Courchevel area compared with the SAR output image of this area

The left image shows the flightpath (yellow line) on the DEM that was used for this analysis. The right figure shows the SAR result as generated by the radar simulator. The legend bar shows the height of the ground above MSL in meters. This flight had a duration of 125 seconds with an average velocity of 97 knots TAS. The total flight distance was 6238 meters. The straight black lines perpendicular to the direction of the flightpath indicate the upper and lower limits of the SAR image. The Y-axis on the SAR image therefore equals the flightpath, or the aircraft longitudinal axis. The noise that is present on low range values in the SAR image are caused by the fact that these groundpoints are too close to the aircraft to be seen. The radar can detect the ground approximately 38 degrees below the local horizontal due to the radar gain profile (Figure 5-6, Appendix B).

When looking at the range between 1500 and 5000 meters, where there is no noise present, the amount of echo points with useful data can be analyzed. Between 1500 and 5000 meters, the radar checks for data every 5 meters, or 700 times. For each array of 700 ranges the radar gets a DEM echo on average for 119 points, or 17% of the time. When looking at the amount of DEM points that are expected to be present in each array, the expected value is 168 points (spacing of 20.84 meters for a 3500 meter range). This means that 71% of the points on the DEM are detected by the radar in this image.

Figure 6-4 correspond to what was expected showing the applicability of the CAR in SAR mode in mountainous terrain. However, because of the resolution of the DEM and the absence of building-like objects, another self developed DEM has been used to analyse the results of the CAR in SAR mode.

6-2-2 Results of the SAR using a created DEM

The results of the SAR image of the DEM that was manually created are obtained by logging a manual flight in X-Plane 10. The average velocity was 99 knots TAS and with a log frequency of 2Hz the longitudinal resolution is 25.5 meters. The altitude was around 200 meters, which is chosen to correspond with the altitude on downwind leg for a general VFR approach procedure. The original DEM and the corresponding resulting SAR image are shown in Figure 6-5.

The range resolution of the radar remains 5 meters. The longitudinal resolution is dependent on the frequency of the state output from X-Plane 10 and remains 25.5 meters. The resulting data is not interpolated. The color scale of both images is matched so that the comparison is made easier visually. The results are transformed from radar reference frame to aircraft body frame, then translated to a stable reference frame on zero altitude. This translation compensates for any roll, pitch and yaw angles of the aircraft. The color legend denotes distance above ground level in meters.
The radar checks the return signal every 5 meters for the range from 0 to 5000 meters. The highest resolvable resolution is therefore 5 meters. The spacing of the points on the DEM is 3.59 meters. With this resolution, in the range between 300 and 5000 meters, the expected amount of DEM points is 1309. This specific range is chosen because it is certain to be detectable according to the radar gain profile (Appendix B). This exceeds the amount of ranges that the radar resolves, which is 940 different ranges between 300 and 5000 meters with a resolution of 5 meters. Within this range, the radar detects on average 913 points

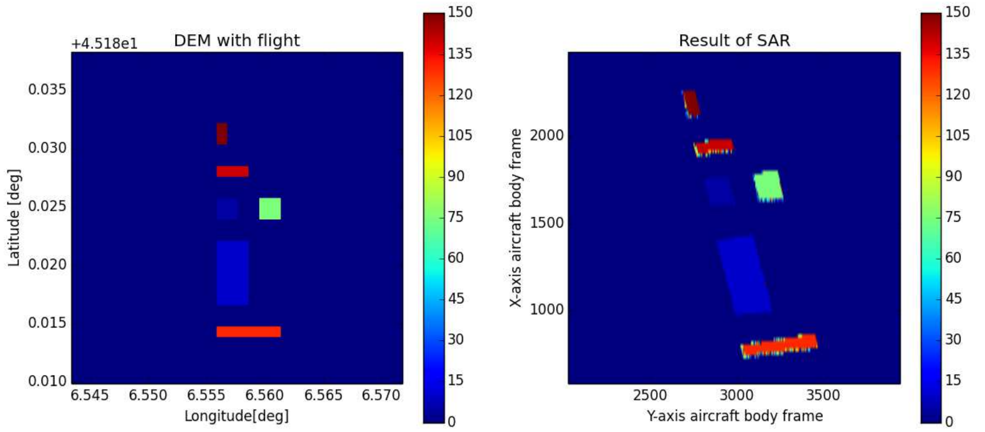

Figure 6-5: Left image shows the original DEM. Right image shows the SAR result obtained with the radar

on the DEM for each range array. This corresponds to a 97% return rate. This means the maximum resolution of 5 meters is achieved for this image.

6-2-3 Stability analysis of body angles

Because state parameters are not exactly known, the radar-ground geometry is subject to inaccuracies. Random noise is induced in the roll, pitch and yaw angles of the aircraft so that the transformation matrix does not exactly compensate for the aircraft body angles. The noise is created using the Numpy random function. Random noise between 0 and 2 degrees, between 0 and 3 degrees and between 0 and 5 degrees is used to create a SAR image of the same self created DEM. The results of adding random noise to the aircraft body angles is shown in Figure 6-6.

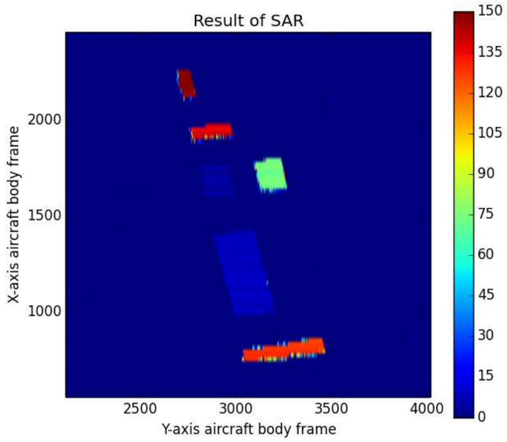

(a) Random noise between 0 and 2 degrees

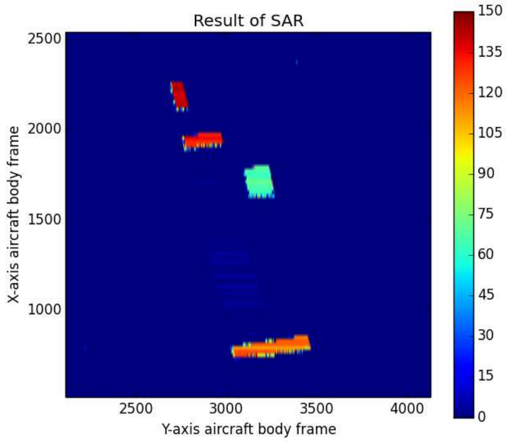

(b) Random noise between 0 and 3 degrees

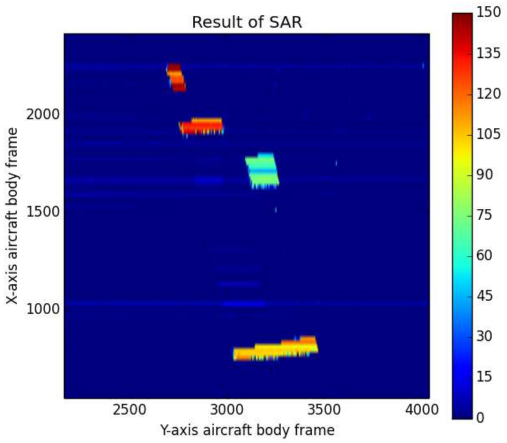

(c) Random noise between 0 and 5 degrees

Figure 6-6: Resulting SAR image with random noise added to the aircraft body angles

Chapter 7

Discussion

7-1 Discussion of the results of the flight simulator experiment

The trend from conditions 1 through 7 is visible in that the deviations become smaller and smaller, which is to be expected since the lateral deviations decrease in conditions 1 through 7. The relative wind direction switches every condition. Every even condition seemed to have higher deviations than the previous odd condition, which indicates that steering against the wind requires a less aggressive manoeuvre.

Condition C8 shows no significant change in roll angle when compared with the base condition. This is to be expected since condition C8 only involved longitudinal overshoot and therefore required no roll correction. It does however fail to retain the null hypothesis of the t-test on the pitch angle. This can be explained by the required increase in negative pitch when the overshoot is detected by the participant.

Conditions 9 through 12 consist of longitudinal overshoot combined with lateral deviations. By analyzing the t-test results of pitch angle θ of conditions 11 and 12, it seems that the null hypothesis is retained for conditions 11 and very close to the threshold on condition 12. The corresponding values are 120 and 60 meters respectively for overshoot and 80 and 120 meters respectively for lateral deviations. This suggests that some overshoot might be acceptable while retaining the null hypothesis on the t-test.

The hypothesis of chapter 4 expected that below 100 meters deviation there would be no significant change in aircraft behavior for correcting manoeuvres. The results of this experiment have falsified this hypothesis, because even a lateral deviation of 40 meters appears to require significant changes in roll behavior to compensate for. The results show that we need a radar system that provides at least a better lateral accuracy than 40 meters and at least a better longitudinal accuracy than 60 meters.

The Cooper-Harper rating scale is designed to provide a subjective rating about the handling qualities of the aircraft. It becomes clear from Table 6-5 that the ratings also correlate positively with the lateral deviation for the first seven conditions; the lowest lateral deviation shows the lowest average Cooper-Harper rating. According to the rating scale, all ratings of 3 or lower signify adequate handling qualities and are satisfactory without improvement. Only condition 7 gets the average rating of exactly 3.0 which leads to the same conclusions as the objective simulator data; a lateral deviation of less than 40 meters is required for a potential navigation system to be used as a landing guidance system.

7-2 Discussion of results of using the radar simulator in SAR mode

The SAR is based on the radar simulator developed at the Delft University of Technology. The radar simulator uses assumptions that inevitably influence the performance of the SAR. The data that is obtained from the radar is based on the reflection of a digital elevation model. The digital elevation model is known in advance in terms of exact coordinates of each point. For this reason, the radar is able to "see" points that would be obscured in a real life situation. Examples of this are areas behind a mountain or the far side of buildings.

The radar uses discrete points to detect the DEM which leads to the potential result of gaps in the data because neither the radar swath nor the ground is continuous. In real life both these elements would be continuous and data losses of this origin would not exist. The effect of this problem is minimized by using interpolation on the terrain and using a higher echo resolution for analysis. Both of these methods compromise the performance of the calculations.

The current data results rely solely on phase and intensity information. The intensity of the echo should be sufficient for detection and depends in part on the reflectivity of the object. The currently used reflectivity model does not depend on material properties of the world. In reality the reflectivity would be necessary to take into account. This could enhance the quality of the SAR data in that different surfaces with no relative elevation can be distinguished, as well as diminish the quality of the SAR data in that some objects remain unseen due to poor reflectivity.

The results show that it is possible to distinguish between different objects and to distinguish between objects and ground on a resolution that seems high enough for real world objects. However, multiple reflections that could occur between ground and objects are not taken into account. In reality these reflections could induce noise in the system that make it harder to distinguish between different objects and the ground.

The results are based on the assumption that there is no ambiguity in the phase difference between multiple antennas. However, this assumption is only valid if the distance between the antennas is smaller than one wavelength. For the simulator this requirement is met, but in reality it is impossible due to the physical size of the antenna. This means that a solution must be found to deal with the ambiguity in phase difference. This problem is not considered part of this research.

For the SAR to yield a stable image, the echo data is transformed using a transformation matrix that compensates for the aircraft body angles. The random noise analysis for the aircraft body angles shows that with a 2°uncertainty in all states the result is still accurate enough to yield an accuracy of 5 meters; the lowest building in the DEM. With noise of 3°and higher the smallest objects on the DEM start to blend in with the background. State uncertainty is always present in real situations and this might limit the accuracy of the radar.

Using these results, a theoretical depiction of the SAR coverage of a real airfield when flying the VFR traffic circuit is possible. A standard VFR circuit on the Dutch airport EHLE (Lelystad airport) is flown at 700 ft altitude on downwind leg. Given the specifications of the radar and the range results of the SAR on this altitude would yield a radar coverage as shown by the gray area in Figure 7-1. The large blue rectangle represents the VFR circuit around this airport. The grey area is the coverage of the SAR. The SAR coverage is off-set from the downwind leg because of the radar gain profile, where the radar in its current configuration is not able to look further down than $-38°$.

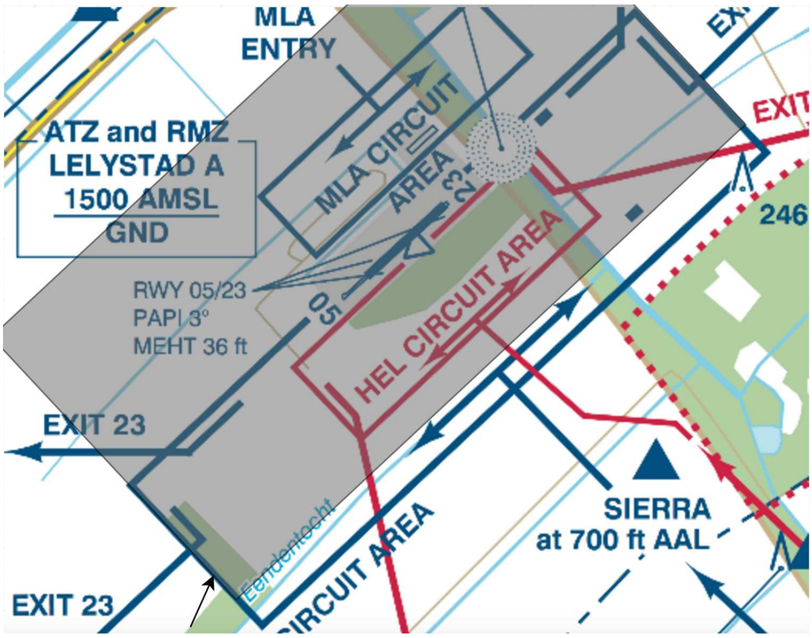

Figure 7-1: The theoretical SAR coverage on Lelystad airport on downwind leg at 700 ft altitude

The range of the radar is sufficient to map the airport on base leg with a resolution of 5 meters. On final leg the SAR does not yield information about the objects of the airport.
The theoretical SAR coverage over Lelystad airport shows that given the normal VFR traffic circuit, the airport is in range of the SAR and objects should be detectable with the specified accuracy. Based on the flight experiment results, the blind time on final leg until reaching the lower cloud base of 200 ft is about one minute. During this time deviations may start

to accumulate. This problem could be minimized by adjusting the VFR traffic circuit as to descend earlier on downwind leg to minimize the blind time on final leg.

All results presented in this thesis are theoretical and not based on real world measurements. Radar information from actual flight experiments should be used and examined to find results on the applicability of the SAR module in real life.

Chapter 8

Conclusion

The goal of this thesis was to investigate the possibility of using a collision avoidance radar (CAR) in a synthetic aperture mode to support the landing procedure in low visibility conditions. The visibility conditions used for this study were equal to those of a CAT I ILS approach.

Human-in-the-loop experiments with relatively untrained pilots in a typical GA aircraft (Cessna 172) show that with CAT I conditions and a crosswind of 10 kts with a gust of 5 kts the lateral deviation should be less than 40 meters with respect to the runway centerline at the decision height and the longitudinal overshoot should be less than 60 meters with respect to the ideal touchdown point at the decision height.

The radar simulator for the CAR has been modified to support the synthetic aperture mode. Using SAR interferometry to obtain range and azimuth information of each point in a DEM the results show that the radar is capable of achieving the maximum resolution of 20.84 meters using a DEM of the Courchevel area from the NASA SRTM mission. With a custom DEM that consisted of predefined building-like objects a resolution of 5 meters was obtained which was the maximum possible resolution due to the range bin resolution of the radar.

The radar in SAR mode amply provides the accuracy requirement of at least 40 meters that was found in the flight experiment. In this exploratory study no evidence was found against the possibility of using the CAR in SAR mode for navigation purposes with an accuracy that exceeds the requirement of CAT I ILS navigation systems. The accuracy limitation of the DEM resolution is resolved when using real world data where the terrain is continuous. In such a situation the accuracy is theoretically only limited by the wavelength of the radar signal.

Chapter 9

Recommendations

9-1 Recommendations regarding the flight experiment

This thesis provides a first set-up for the implementation of the CAR in SAR mode. The approach contains multiple assumptions that should be taken into account, and further research on these assumptions might be warranted for a thorough investigation of the possibilities of using radar in approach and landing procedures. Therefore, several of these assumptions and corresponding recommendations will be discussed in this chapter.

The flight experiment study on the required accuracy of a navigation module consisted of twelve participants. Parametric statistical tests gain power with larger samples. Also, the range of experiences of the participants could be more strict which results in a more homogeneous sample. Enhancing simulator fidelity can further improve the results, because participants will be less likely to overestimate their abilities and underestimate dangerous situations in a high fidelity simulator.

The results of the flight experiment are not conclusive about the accuracy requirements regarding the lateral and longitudinal deviations at 200 ft altitude with a Cessna 172 aircraft. In order to get a better specification of these requirements the conditions should be altered to consider much smaller deviations. A suggestion might be to use the smallest deviation of this study and get closer to zero meters deviation.

This thesis used the conventional VFR approach procedure and developed a system that depends on the limitations of this procedure. Future research on this subject might consider altering the approach procedures in such a way that the 'blind time' on final leg is reduced to a minimum. For example, the aircraft might descend towards the lower cloud base while on base leg so that visual information is already available when turning to final leg.

9-2 Recommendations regarding the implementation of SAR

The radar simulator uses reception antennas that are closer together than one wavelength. In reality this is not possible due to the physical size of the antennas. This leads to an ambiguity when using radar interferometry because the phase difference between the two antennas can be shifted a full wavelength. This ambiguity is not solved for this particular problem and an algorithm could be developed that considers each solution to the equation and finds the best fit.

Another possibility is to change the data processing method as it is currently implemented. The data processing method used in this thesis relies on radar interferometry to compare the phase difference between two reception antennas for the direction of the signal, and uses time delay between transmission and reception to determine the range. There are other methods conceivable for processing radar data in order to get high resolution images (Meta et al., 2007) (Chan & Koo, 2008). However, the radar simulator might require more adjustments which could possibly conflict with its current purpose as collision avoidance and obstacle detection radar.

The radar processor analyzes information about phase and intensity of the return signal. The intensity depends on the reflectivity of the surface. The radar simulator uses a simple reflectivity model that does not account for variations in material, only in relative angle with respect to the radar. Reflectivity of different materials and multiple reflections caused by ground-object interference will add another dimension to the processing of real data. Actual radar data from flight experiments could provide valuable insight in the capabilities of developing a radar-based navigation system.

The resulting image of the SAR could potentially yield accurate information about objects on the ground. In order to be able to navigate using SAR, seen objects should be compared with a known object database. Currently, all digital elevation models considered in this research do not contain information about man-made objects. Other certified sources should be consulted that contain up-to-date information about ground objects or landmarks that could be used for navigation using a radar-based navigation system.

Using the SAR images for position determination, this information can be translated to guide the pilot towards his destination. This would require a graphical user interface that intuitively presents information about any deviations from the desired flight path. Such a design could be integrated in a synthetic vision system using a tunnel-in-the-sky.

Appendix A

Statistical analysis of X-Plane 10 flight data

This appendix shows the parts of the code that transform raw X-Plane 10 output data to results of the statistical analysis.

The following code reads in the .txt file outputted by X-Plane 10 and extracts the relevant variables. The column numbers corresponding to variables may differ when another set of output variables is chosen in X-Plane 10.

```
# Importing the datafiles using the relevant columns for the experiment into a Numpy array
def read_datafile(file_name):
    data = np.loadtxt(file_name, delimiter = '|', skiprows = 2, usecols = (2, 7, 16, 17,
    18, 26, 27, 28, 37, 38, 39, 40, 41, 42, 43, 44, 45, 47, 54, 60, 61, 62, 71, 72, 73,
     75, 76))
    # columns:
    # 2 --> 0 - Mission time
    # 7 --> 1 - IAS [kts]
    # 16 --> 2 - G Load (normal) [G]
    # 17 --> 3 - G Load (axial) [G]
    # 18 --> 4 - G Load (side) [G]
    # 26 --> 5 - Elevator yoke
    # 27 --> 6 - Aileron yoke
    # 28 --> 7 - Rudder yoke
    # 37 --> 8 - Pitch moment M
    # 38 --> 9 - Roll moment L
    # 39 --> 10 - Yaw moment N
    # 40 --> 11 - Pitch derivative
    # 41 --> 12 - Roll derivative
    # 42 --> 13 - Yaw derivative
    # 43 --> 14 - Pitch
    # 44 --> 15 - Roll
    # 45 --> 16 - Heading
    # 47 --> 17 - AoA
    # 54 --> 18 - Alt MSL
    # 60 --> 19 - X
    # 61 --> 20 - Y
    # 62 --> 21 - Z
    # 71 --> 22 - gear1
    # 72 --> 23 - gear2
    # 73 --> 24 - gear3
    # 75 --> 25 - CL
    # 76 --> 26 - CD


    # Find when the actual situation is loaded, and discard data that was outputted
    # before the experiment situation was started
    item1 = 0.0
```

```
    for index, item in enumerate(data[:,0]):
        item2 = item
        if item2 < item1:
            # delete everything up to this point from list
            data = data[index:,:]
            break
        else:
            item1 = item2

    return data
```

The following code analyzes all the base conditions of all participants with the crosswind component. This forms the baseline for analysis. Only the data is used on final leg on the part where participants are required to perform a correcting manoeuvre. All the analyzed data for the flight variables are those before touchdown, because after touchdown variables such as angle of attack may show significant amounts of noise. The extreme values in this phase of flight are stored for analysis.

```
# Analysis of all the base conditions with crosswind
for i in range(1, 13):
    for j in range(2,3):
        filename = 'P' + str(i) + 'B' + str(j) + '.txt'
        data = read_datafile(filename)

        x = data[:,0]
        V_ias = data[:,1]
        G_nrm = data[:,2]
        G_ax = data[:,3]
        G_side = data[:,4]
        El_yoke = data[:,5]
        Ail_yoke = data[:,6]
        Rud_yoke = data[:,7]
        M = data[:,8]
        L = data[:,9]
        N = data[:,10]
        q = data[:,11]
        p = data[:,12]
        r = data[:,13]
        theta = data[:,14]
        phi = data[:,15]
        psi = data[:,16]
        alpha = data[:,17]
        h_msl = data[:,18]
        loc_x = data[:,19]
        loc_y = data[:,20]
        loc_z = data[:,21]
        gearforce1 = data[:,22]
        gearforce2 = data[:,23]
        gearforce3 = data[:,24]
        cL = data[:,25]
        cD = data[:,26]

        # array with the three strut forces combined
        gearforce_total = np.empty([0,0])
        gearforce_total = np.append(gearforce_total, [gearforce1, gearforce2, gearforce3])

        # Determine location of touchdown
        for index, item in enumerate(gearforce1):
            if item > 0:
                index_gear1 = index
                break
        for index, item in enumerate(gearforce2):
            if item > 0:
                index_gear2 = index
                break
        for index, item in enumerate(gearforce3):
            if item > 0:
                index_gear3 = index
                break

        if index_gear2 < index_gear1:
            if index_gear3 < index_gear2:
                index_touchdown = index_gear3
            else:
                index_touchdown = index_gear2
        elif index_gear1 < index_gear3:
            index_touchdown = index_gear1
        else:
            index_touchdown = index_gear3

        # Calculate extreme values from dataset on final leg
```

```
#       Check where decision height is reached, altitude below 220ft
#       for index, item in enumerate(h_msl):
#           if item < 220:
#               for a in range(0,index):
#                   data_final = np.delete(data, np.s_[::index], axis=0)
#                   data_final = data[index:,:]
#               break
#       Ok, so for now we dont use cloudbase, just calculate back 30 seconds from touchdown
#       point to ensure same length vectors for all variables
        index = index_touchdown - 150

        x_base = data[index:index_touchdown:1,0] # time vector

        Vias_base = data[index:index_touchdown:1,1] # knots indicated airspeed
        theta_base = data[index:index_touchdown:1,14] # pitch angle
        q_base = data[index:index_touchdown:1,11] # pitch derivative
        M_base = data[index:index_touchdown:1,8] # pitch moment
        phi_base = data[index:index_touchdown:1,15] # roll angle
        p_base = data[index:index_touchdown:1,12] # roll derivative
        L_base = data[index:index_touchdown:1,9] # roll moment
        r_base = data[index:index_touchdown:1,13] # yaw derivative
        N_base = data[index:index_touchdown:1,10] # yaw moment
        G_nrm_base = data[index:index_touchdown:1,2] # normal g load
        G_ax_base = data[index:index_touchdown:1,3] # axial g load
        G_side_base = data[index:index_touchdown:1,4] # side g load
        Ail_yoke_base = data[index:index_touchdown:1,6] # aileron yoke
        El_yoke_base = data[index:index_touchdown:1,5] # elevator yoke
        for index2, item in enumerate(h_msl):
            if item < 30.0:
                AoA_base = alpha[index:index2:1]
                break

        # Touchdown location:
        x_tchdwn_base = data[index_touchdown,19]
        z_tchdwn_base = data[index_touchdown,21]
        x_dev_base = np.abs(x_land - x_tchdwn_base)
        z_dev_base = np.abs(z_land - z_tchdwn_base)

#       Determine extreme values per flight
        thetamax_base = np.append(thetamax_base, np.max(np.abs(theta_base)))
        qmax_base = np.append(qmax_base, np.max(np.abs(q_base)))
        Mmax_base = np.append(Mmax_base, np.max(np.abs(M_base)))
        phimax_base = np.append(phimax_base, np.max(np.abs(phi_base)))
        pmax_base = np.append(pmax_base, np.max(np.abs(p_base)))
        Lmax_base = np.append(Lmax_base, np.max(np.abs(L_base)))
        rmax_base = np.append(rmax_base, np.max(np.abs(r_base)))
        Nmax_base = np.append(Nmax_base, np.max(np.abs(N_base)))
        G_nrm_base = np.append(G_nrm_base, np.max(np.abs(G_nrm_base)))
        G_ax_base = np.append(G_ax_base, np.max(np.abs(G_ax_base)))
        G_side_base = np.append(G_side_base, np.max(np.abs(G_side_base)))
        AoAmax_base = np.append(AoAmax_base, np.max(np.abs(AoA_base)))
        gearforce_max_base = np.append(gearforce_max_base, np.max(np.abs(gearforce_total)))
        tchdwn_dev_max_base = np.append(tchdwn_dev_max_base, sqrt(pow(x_dev_base,2) + pow(z_dev_base
            ,2)))
        Ail_yoke_max_base = np.append(Ail_yoke_max_base, np.max(np.abs(Ail_yoke_base)))
        El_yoke_max_base = np.append(El_yoke_max_base, np.max(np.abs(El_yoke_base)))
```

The following code does the same analysis for each of the test conditions. Only the code for the first test condition is shown. All other test conditions use the exact same assertions.

```
# Analysis of the actual test conditions
for i in range(1, 13): # conditions
    for j in range(1,13): # participants
        filename = 'P' + str(j) + 'C' + str(i) + '.txt'
        data = read_datafile(filename)

        x = data[:,0]
        V_ias = data[:,1]
        G_nrm = data[:,2]
        G_ax = data[:,3]
        G_side = data[:,4]
        El_yoke = data[:,5]
        Ail_yoke = data[:,6]
        Rud_yoke = data[:,7]
        M = data[:,8]
        L = data[:,9]
        N = data[:,10]
        q = data[:,11]
        p = data[:,12]
        r = data[:,13]
        theta = data[:,14]
        phi = data[:,15]
        psi = data[:,16]
        alpha = data[:,17]
        h_msl = data[:,18]
        loc_x = data[:,19]
        loc_y = data[:,20]
        loc_z = data[:,21]
```

```
gearforce1 = data[:,22]
gearforce2 = data[:,23]
gearforce3 = data[:,24]
cL = data[:,25]
cD = data[:,26]

# array with the three strut forces combined
gearforce_total = np.empty([0,0])
gearforce_total = np.append(gearforce_total, [gearforce1, gearforce2, gearforce3])

# Determine location of touchdown
for index, item in enumerate(gearforce1):
    if item > 0:
        index_gear1 = index
        break
for index, item in enumerate(gearforce2):
    if item > 0:
        index_gear2 = index
        break
for index, item in enumerate(gearforce3):
    if item > 0:
        index_gear3 = index
        break

if index_gear2 < index_gear1:
    if index_gear3 < index_gear2:
        index_touchdown = index_gear3
    else:
        index_touchdown = index_gear2
elif index_gear1 < index_gear3:
    index_touchdown = index_gear1
else:
    index_touchdown = index_gear3

# Calculate extreme values from dataset on final leg

# Check where decision height is reached, altitude below 220ft
#       for index, item in enumerate(h_msl):
#           if item < 220:
#               for b in range(0,index):
#   #               data_final = np.delete(data, np.s_[::index], axis=0)
#                   data_final = data[index:,:]
#               break
#       Ok, so for now we dont use cloudbase, just calculate back 30 seconds from touchdown
#       point to ensure same length vectors for all variables
index = index_touchdown - 150

x_c = data[index:index_touchdown:1,0] # time vector

Vias_c = data[index:index_touchdown:1,1] # knots indicated airspeed
theta_c = data[index:index_touchdown:1,14] # pitch angle
q_c = data[index:index_touchdown:1,11] # pitch derivative
M_c = data[index:index_touchdown:1,8] # pitch moment
phi_c = data[index:index_touchdown:1,15] # roll angle
p_c = data[index:index_touchdown:1,12] # roll derivative
L_c = data[index:index_touchdown:1,9] # roll moment
r_c = data[index:index_touchdown:1,13] # yaw derivative
N_c = data[index:index_touchdown:1,10] # yaw moment
G_nrm_c = data[index:index_touchdown:1,2] # normal g load
G_ax_c = data[index:index_touchdown:1,3] # axial g load
G_side_c = data[index:index_touchdown:1,4] # side g load
Ail_yoke_c = data[index:index_touchdown:1,6] # aileron yoke
El_yoke_c = data[index:index_touchdown:1,5] # elevator yoke
for index2, item in enumerate(h_msl):
    if item < 30.0:
        AoA_c = alpha[index:index2:1]
        break

# Touchdown location:
x_tchdwn_c = data[index_touchdown,19]
z_tchdwn_c = data[index_touchdown,21]
x_dev_c = np.abs(x_land - x_tchdwn_c)
z_dev_c = np.abs(z_land - z_tchdwn_c)

#       Determine extreme values per flight per condition
if i == 1:
    thetamax_c1 = np.append(thetamax_c1, np.max(np.abs(theta_c)))
    qmax_c1 = np.append(qmax_c1, np.max(np.abs(q_c)))
    Mmax_c1 = np.append(Mmax_c1, np.max(np.abs(M_c)))
    phimax_c1 = np.append(phimax_c1, np.max(np.abs(phi_c)))
    pmax_c1 = np.append(pmax_c1, np.max(np.abs(p_c)))
    Lmax_c1 = np.append(Lmax_c1, np.max(np.abs(L_c)))
    rmax_c1 = np.append(rmax_c1, np.max(np.abs(r_c)))
    Nmax_c1 = np.append(Nmax_c1, np.max(np.abs(N_c)))
    G_nrm_max_c1 = np.append(G_nrm_max_c1, np.max(np.abs(G_nrm_c)))
    G_ax_max_c1 = np.append(G_ax_max_c1, np.max(np.abs(G_ax_c)))
    G_side_max_c1 = np.append(G_side_max_c1, np.max(np.abs(G_side_c)))
    AoAmax_c1 = np.append(AoAmax_c1, np.max(np.abs(AoA_c)))
    gearforce_max_c1 = np.append(gearforce_max_c1, np.max(np.abs(gearforce_total)))
    tchdwn_dev_max_c1 = np.append(tchdwn_dev_max_c1, sqrt(pow(x_dev_c,2) + pow(z_dev_c,2)))
```

```
    Ail_yoke_max_c1 = np.append(Ail_yoke_max_c1, np.max(np.abs(Ail_yoke_c)))
    El_yoke_max_c1 = np.append(El_yoke_max_c1, np.max(np.abs(El_yoke_c)))
```

Using the maximum values for all conditions and the base condition for all participants, the boxplots can be created that show the distribution of these variables. The code for one variable is shown. For each variable the code is repeated.

```
# Boxplots
plt.figure()
plt.boxplot([phimax_base, phimax_c1, phimax_c2, phimax_c3, phimax_c4, phimax_c5,
phimax_c6, phimax_c7, phimax_c8, phimax_c9, phimax_c10, phimax_c11, phimax_c12])
plt.xticks([1,2,3,4,5,6,7,8,9,10,11,12,13], ['Base', '1', '2', '3', '4', '5', '6', '7',
 '8', '9', '10', '11', '12'])
plt.xlabel("Condition")
plt.ylabel("Roll angle [Degrees]")
plt.title('Roll angle')
```

Appendix B

Radar gain profile

The following figures provide information about the gain profile of the main lobe and side lobes of the radar for varying azimuth and elevation angles. Azimuth information if provided in Figure B-1 and elevation information is provided in Figure B-2.

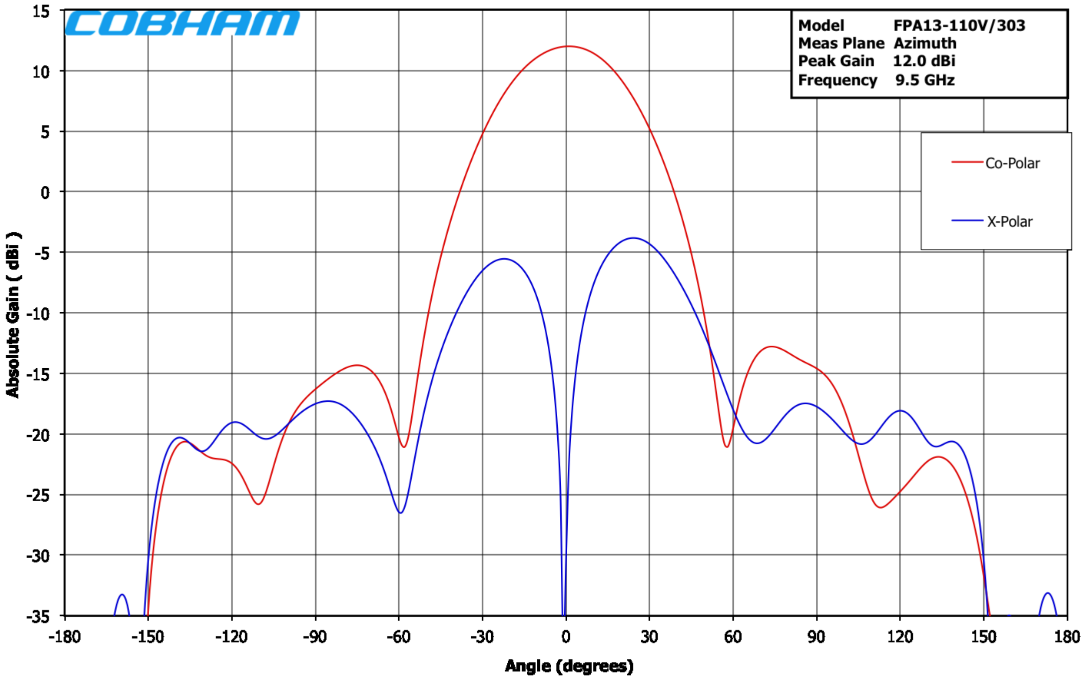

Figure B-1: Radar gain profile with varying azimuth angle

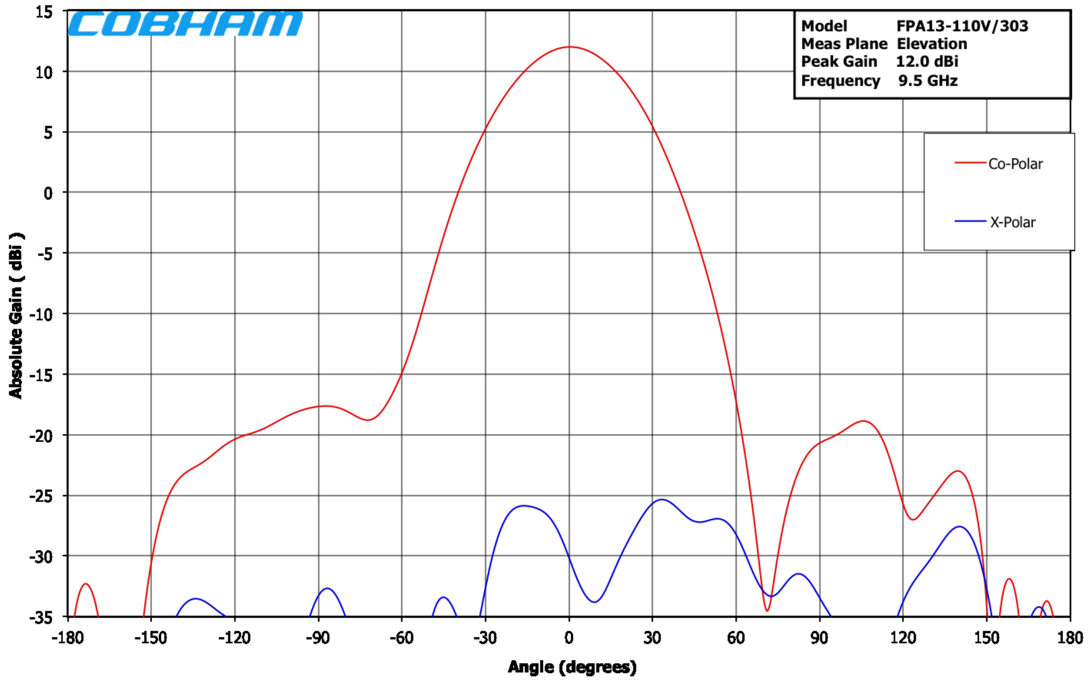

Figure B-2: Radar gain profile with varying elevation angle

Appendix C

Boxplot results of all variables

The thesis shows the results and analysis of the roll angle ϕ, pitch angle θ and angle of attack α. This appendix shows for sake of completeness the results of all boxplots that resulted from the analysis of the variables.

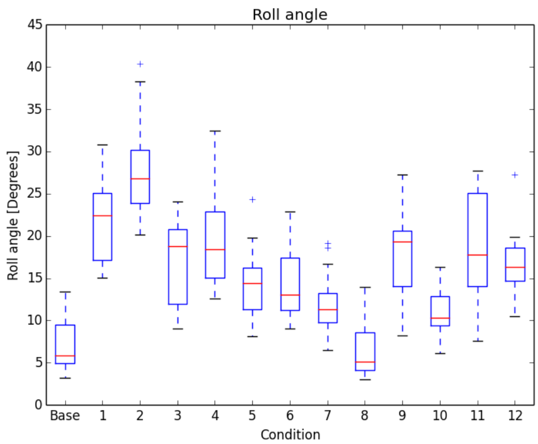

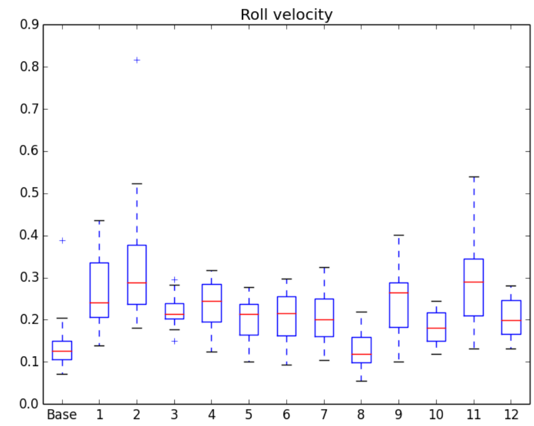

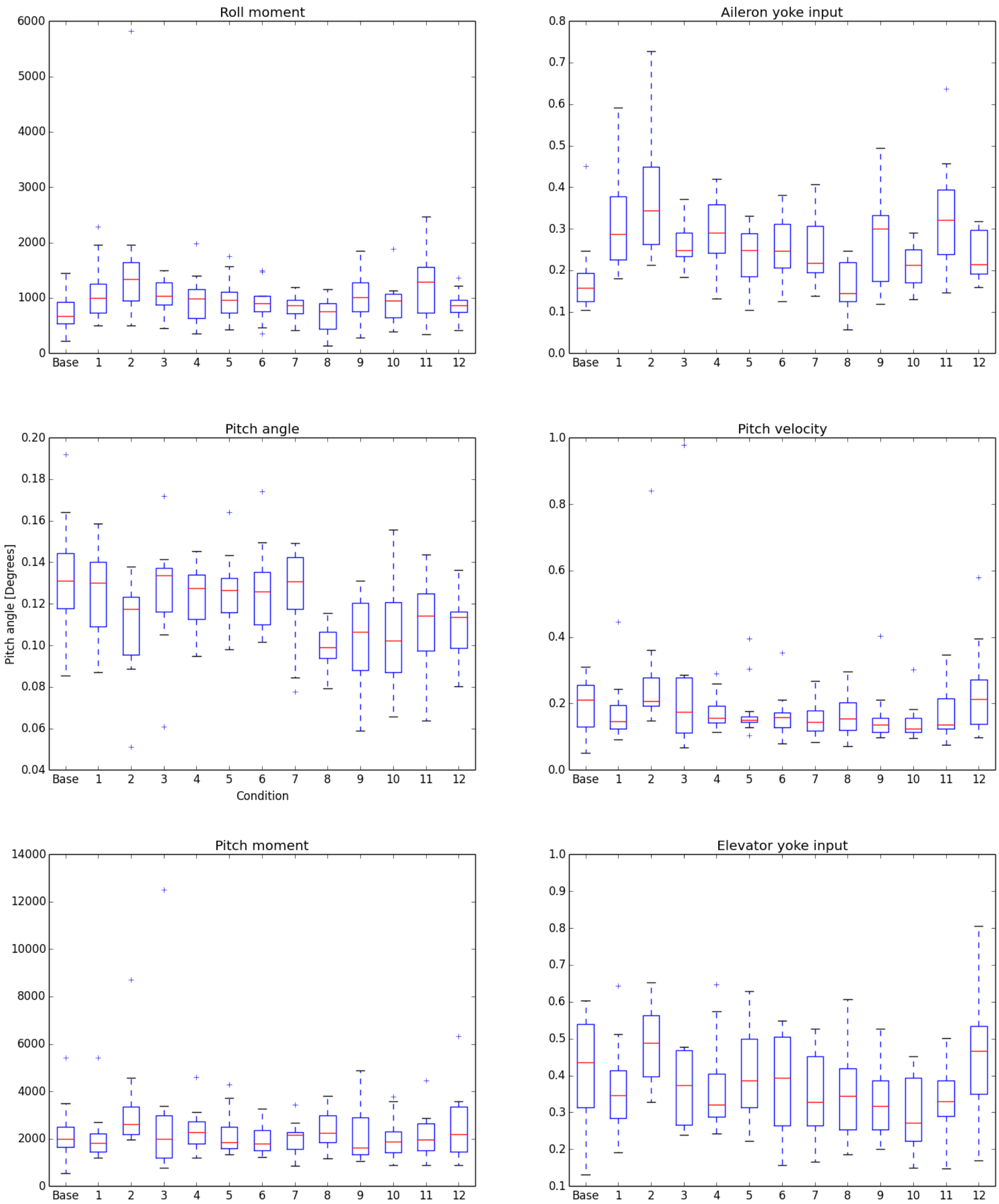
Roll moment
Aileron yoke input
Pitch angle
Pitch angle [Degrees]
Condition
Pitch velocity
Pitch moment
Elevator yoke input
Base 1 2 3 4 5 6 7 8 9 10 11 12

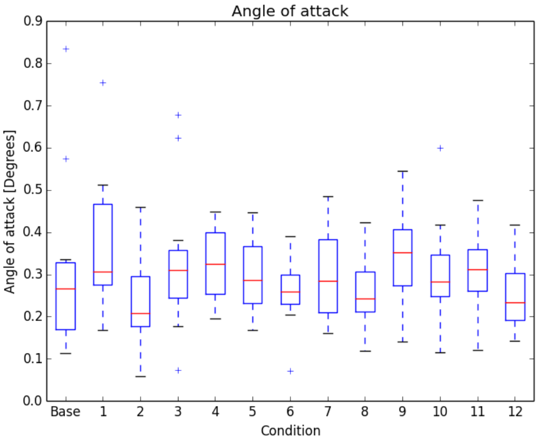
Angle of attack
Angle of attack [Degrees]
Condition
Base 1 2 3 4 5 6 7 8 9 10 11 12

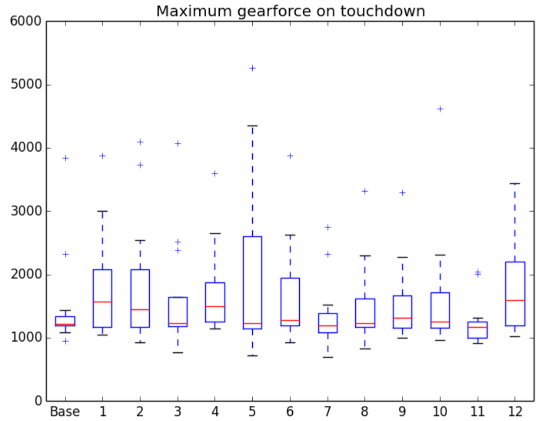
Maximum gearforce on touchdown
Base 1 2 3 4 5 6 7 8 9 10 11 12

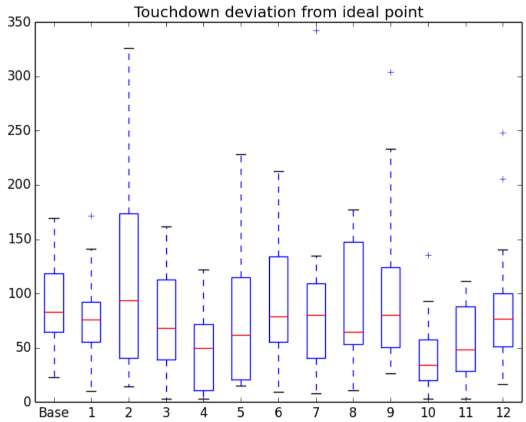
Touchdown deviation from ideal point
Base 1 2 3 4 5 6 7 8 9 10 11 12

Appendix D

Radar simulator and SAR module code

The radar processor is confidential information and is not included in this version of the thesis. For more information on this part, please contact the Delft University of Technology.

Appendix E

State data of the flights used for the radar

The flight that was used for the SAR simulations was a manually flown flight in X-Plane 10 and the output data was used to simulate the radar. The state variables with respect to time are presented here for an understanding of the stability of the used flight. The data was obtained by writing a Python program for data extraction. The code for the program is presented here:

```python
"""
Author: Laurens Baardman
Modified: 06-08-2016
"""

import sys
import os

import matplotlib as mpl
mpl.use('TKagg') # Necessary for the back-end to work properly
import matplotlib.pyplot as plt
from matplotlib.ft2font import FT2Font
from matplotlib.font_manager import FontProperties
from mpl_toolkits.mplot3d import Axes3D
import numpy as np

def read_datafile(file_name):
    data = np.loadtxt(file_name, delimiter = '|', skiprows = 20, usecols = (2, 7, 16, 17,
    18, 26, 27, 28, 37, 38, 39, 40, 41, 42, 43, 44, 45, 47, 54, 60, 61, 62, 71, 72, 73,
     75, 76))
    # columns:
    # 2 --> 0 - Mission time
    # 7 --> 1 - IAS [kts]
    # 16 --> 2 - G Load (normal) [G]
    # 17 --> 3 - G Load (axial) [G]
    # 18 --> 4 - G Load (side) [G]
    # 26 --> 5 - Elevator yoke
    # 27 --> 6 - Aileron yoke
    # 28 --> 7 - Rudder yoke
    # 37 --> 8 - Pitch moment M
    # 38 --> 9 - Roll moment L
    # 39 --> 10 - Yaw moment N
    # 40 --> 11 - Pitch derivative
    # 41 --> 12 - Roll derivative
    # 42 --> 13 - Yaw derivative
    # 43 --> 14 - Pitch
    # 44 --> 15 - Roll
    # 45 --> 16 - Heading
    # 47 --> 17 - AoA
    # 54 --> 18 - Alt MSL
    # 60 --> 19 - X
    # 61 --> 20 - Y
    # 62 --> 21 - Z
```

```python
    # 71 --> 22 - gear1
    # 72 --> 23 - gear2
    # 73 --> 24 - gear3
    # 75 --> 25 - CL
    # 76 --> 26 - CD


    # Find when the actual situation is loaded, and discard data that was outputted
    # before the experiment situation was started
    item1 = 0.0
    for index, item in enumerate(data[:,0]):
        item2 = item
        if item2 < item1:
            # delete everything up to this point from list
            data = data[index:,:]
            break
        else:
            item1 = item2

    return data

flightdata = read_datafile("courchevel4.txt")
time = flightdata[:,0]
IAS = flightdata[:,1]
theta = flightdata[:,14]
dtheta = flightdata[:,11]
dtheta = np.rad2deg(dtheta)
phi = flightdata[:,15]
dphi = flightdata[:,12]
dphi = np.rad2deg(dphi)
heading = flightdata[:,16]
dheading = flightdata[:,13]
dheading = np.rad2deg(dheading)
flightdata[:,18] = 657
alt_msl = flightdata[:,18]

plt.figure()
plt.plot(time, IAS)
plt.xlabel('Time [s]')
plt.ylabel('IAS [kts]')
plt.title('Indicated airspeed')
plt.grid()

plt.figure()
plt.subplot(211)
plt.plot(time, theta)
plt.xlabel('Time [s]')
plt.ylabel('Pitch [deg]')
plt.title('Pitch angle and pitch rate')
plt.grid()
plt.subplot(212)
plt.plot(time, dtheta)
plt.xlabel('Time [s]')
plt.ylabel('Pitch rate [deg/s]')
plt.grid()

plt.figure()
plt.subplot(211)
plt.plot(time, phi)
plt.xlabel('Time [s]')
plt.ylabel('Roll [deg]')
plt.title('Roll angle and roll rate')
plt.grid()
plt.subplot(212)
plt.plot(time, dphi)
plt.xlabel('Time [s]')
plt.ylabel('Roll rate [deg/s]')
plt.grid()

plt.figure()
plt.subplot(211)
plt.plot(time, heading)
plt.xlabel('Time [s]')
plt.ylabel('Heading [deg]')
plt.title('Heading and yaw rate')
plt.grid()
plt.subplot(212)
plt.plot(time, dheading)
plt.xlabel('Time [s]')
plt.ylabel('Yaw rate [deg/s]')
plt.grid()

plt.figure()
plt.plot(time, alt_msl)
plt.xlabel('Time [s]')
plt.ylabel('Alt MSL [ft]')
plt.title('Altitude above MSL')
plt.grid()
plt.show()
```

The results for the flight over Courchevel area:

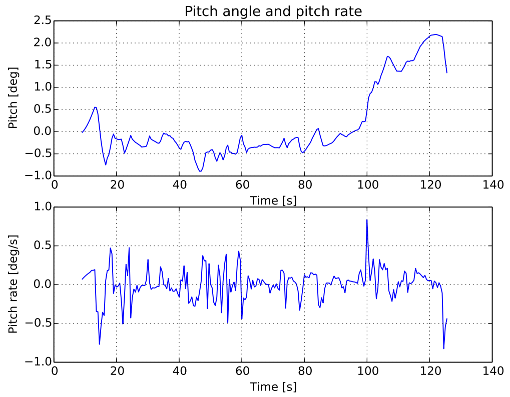

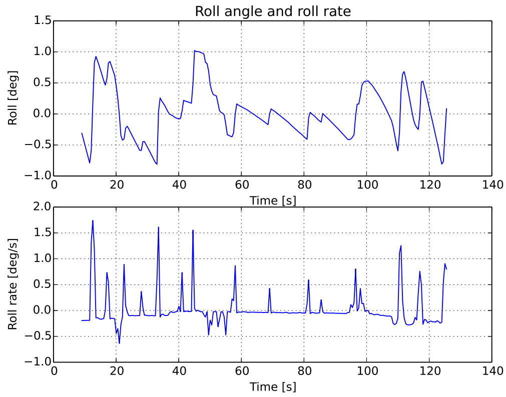

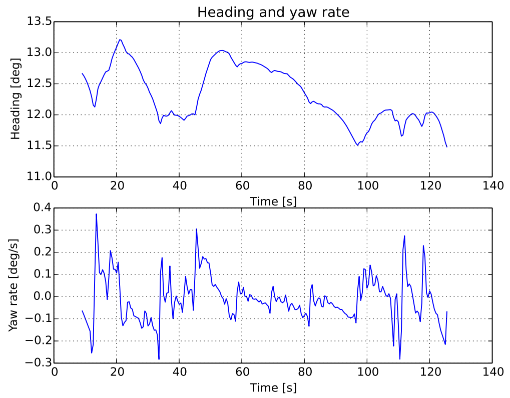

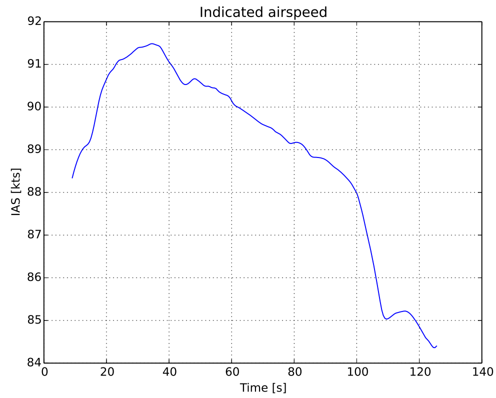

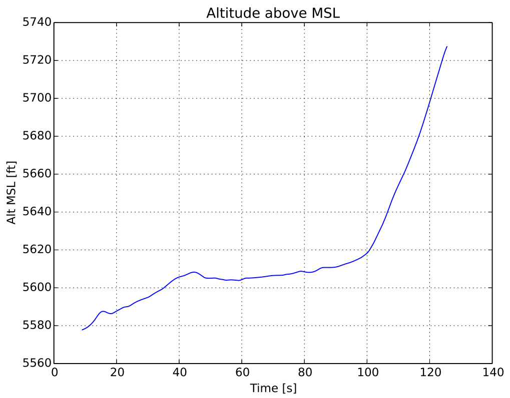

The results for the flight with the self created DEM:

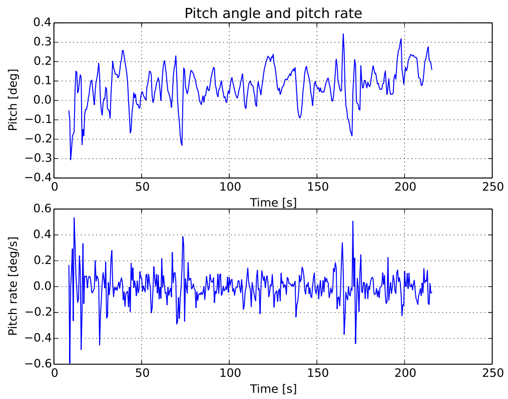

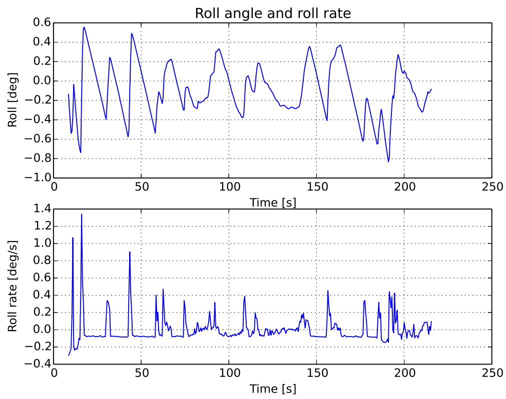

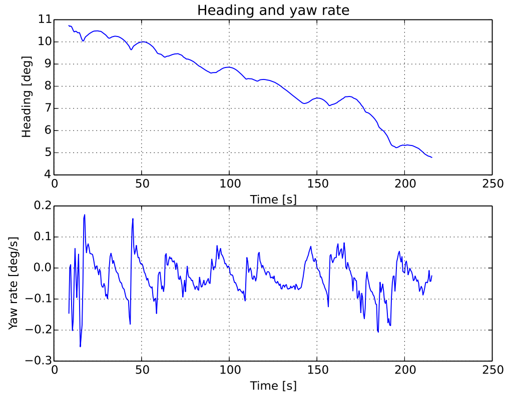

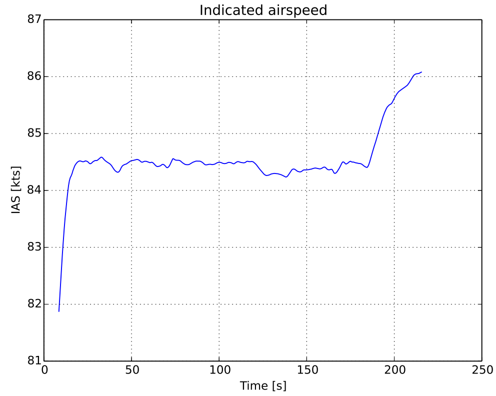

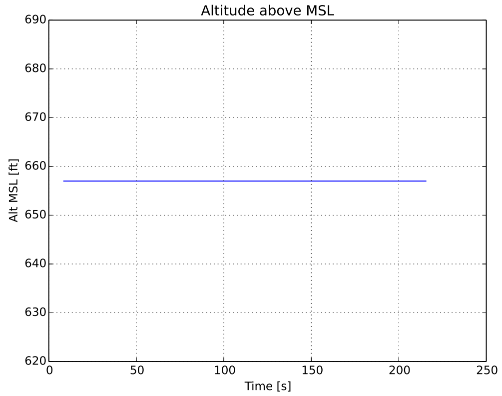

Bibliography

Chan, Y., & Koo, V. (2008). An Introduction to Synthetic Aperture Radar (SAR). *Progress In Electromagnetics Research B*, *2*(6), 27–60. Available from http://content.apa.org/reviews/008772

Cooper, G. E., & Harper, R. P. (1969). *The use of pilot rating in the evaluation of aircraft handling qualities* (Tech. Rep. No. April). Washington, United States: NASA Ames Research Center; Moffett Field, CA, United States.

Diana, T. (2015). Is access to general aviation airports with precision approach and no instrument landing systems a club good? A study of six airports. *Case Studies on Transport Policy*, *3*(2), 238–242. Available from http://www.scopus.com/inward/record.url?eid=2-s2.0-84929833226&partnerID=tZOtx3y1

El-Rabbany, A. (2002). *Introduction to gps : the global positioning system.* Boston, MA :: Artech House,.

Hwang, P. Y., McGraw, G. A., & Bader, J. R. (1999). Enhanced differential gps carrier-smoothed code processing using dual-frequency measurements. , *46*(2), 127-137.

Hyun, E., Kim, S.-D., Ju, Y.-H., Lee, J.-H., You, E.-N., Park, J.-H., et al. (2011). FPGA based signal processing module design and implementation for FMCW vehicle radar systems. *Proceedings of 2011 IEEE CIE International Conference on Radar*, *1*, 273–275.

Hyun, E., Oh, W., & Lee, J.-H. (2012). Multi-target detection algorithm for FMCW radar. *Radar Conference (RADAR), 2012 IEEE*, 338–341.

Hyun, E. H. E., Oh, W. O. W., & Lee, J.-H. L. J.-H. (2010). Two-Step Moving Target Detection Algorithm for Automotive 77 GHz FMCW Radar. *Vehicular Technology Conference Fall (VTC 2010-Fall), 2010 IEEE 72nd*.

International Civil Aviation Organization Annex 11. (2001). *Annex 11 to the Convention on International Civil Aviation - Air Traffic Services* (No. July).

International Civil Aviation Organization Annex 2. (2005). *Annex 2 to the Convention on International Civil Aviation - Rules of the Air* (No. July). Available from http://www.icao.int/Meetings/anconf12/Document Archive/an02_cons[1].pdf

Kulpa, K. (2001). Novel method of decreasing influence of phase noise on FMCW radar. *CIE International Conference on Radar*

Proceedings (Cat No.01TH8559), *2*(3), 319–323. Available from http://ieeexplore.ieee.org/lpdocs/epic03/wrapper.htm?arnumber=984682

L., Z., & L., Y. G. (2013). Carrier-phase differential gps/ins integrated navigation system. , *760-762*, 457-461.

Loss, K., Nicosia, J., & Taylor, G. (1994). Keith Loss, Joseph Nicosia, Gordon Taylor*. In (pp. 195–198). San Diego, California: Telesystems Conference, 1994. Conference Proceedings., 1994 IEEE National.

Loughin, T. M., Gentleman, R., Carey, V., Huber, W., Irizarry, R., Dudoit, S., et al. (2006). BOOK REVIEWS EDITOR : Bioinformatics and Computational Biology Solutions. (December), 1269–1280.

McKillup, S. (2006). *Statistics explained : an introductory guide for life scientists TT* - (2nd ed. ed.). Cambridge [etc.] :: Cambridge University Press,. Available from http://site.ebrary.com/id/10533274

Meta, A., Hoogeboom, P., & Ligthart, L. P. (2007). Signal processing for FMCW SAR. *IEEE Transactions on Geoscience and Remote Sensing*, *45*(11), 3519–3532.

Naulais, C. (2015). *General Aviation Radar System for Navigation and Attitude Determination.* Unpublished doctoral dissertation, Delft University of Technology.

Nitti, D., Bovenga, F., Chiaradia, M., Greco, M., & Pinelli, G. (2015). Feasibility of Using Synthetic Aperture Radar to Aid UAV Navigation. *Sensors*, *15*(8), 18334–18359. Available from http://www.mdpi.com/1424-8220/15/8/18334/

Ný, V. . Í. Č. (2009). Maximum Available Accuracy of FM-CW Radars. *Radioengineering*, *18*(4), 556–560.

Olkin, I. (1960). *Contributions to probability and statistics : essays in honor of Harold Hotelling TT* -. Stanford, Calif. :: Stanford University Press,. Available from Table of contents http://digitool.hbz-nrw.de:1801/webclient/DeliveryManager?pid=1704233&custom_att_2=simple_viewer http://bvbr.bib-bvb.de:8991/F?func=service&doc_library=BVB01&local_base=BVB01&doc_number=001831963&line_number=0001&func_code=DB_RECORDS&ser

Performance-based Navigation (PBN) Manual. (2008). *International Civil Aviation Organization.*

Raney, R. (1971). Synthetic Aperture Imaging Radar and Moving Targets. *IEEE Transactions on Aerospace and Electronic Systems*, *AES-7*(3), 499–505.

Rohling, H., & Moller, C. (2008). Radar waveform for automotive radar systems and applications. *2008 IEEE Radar Conference*, *1*(1), 1–4. Available from http://ieeexplore.ieee.org/lpdocs/epic03/wrapper.htm?arnumber=4721121

Salih, A. A. A.-A., Zhahir, A., & Ariff, O. K. (2012). Comparative Study on Aircraft Landing Instruments: Accuracies and Limitations. *Applied Mechanics and Materials*, *225*, 549–554. Available from http://www.scientific.net/AMM.225.549

services, T. national technical information. (2005). *Federal Radio and Navigation Plan.* Springfield, Virginia.

Shapiro, S. S., & Wilk, M. B. (1965). An Analysis of Variance Test for Normality (Complete Samples). *Biometrika*, *52*(3/4), 591–611. Available from http://links.jstor.org/sici?sici=0006-3444(196512)52:3/4<591:AAOVTF>2.0.CO;2-B

Skolnik, M. I. (2008). An Introduction and Overview of Radar. In *Radar handbook* (pp. 1.1–1.24).

Soumekh, M. (1994). *Fourier array imaging.* Upper Saddle River, NJ, USA: Prentice-Hall, Inc.

Undheim, R. (2012). *Design of a Linear FMCW Radar Synthesizer with Focus on Phase Noise.* Unpublished doctoral dissertation, Norwegian University of Science and Technology.

Winkler, V. (2007). Range Doppler detection for automotive FMCW radars. In *2007 european radar conference, eurad* (pp. 166–169).

Wojtkiewicz, A., Misiurewicz, J., Nalecz, M., Jedrzejewski, K., & Kulpa, K. (1997). Two-dimensional signal processing in FMCW radars. *Proc. XX-th National Conference on Circuit Theory and Electronic Networks*, *2*(1), 475–480.